Multiple forms of working memory emerge from synapse-astrocyte interactions in a neuron-glia network model

Maurizio De Pittà[a,b,c,d,1] **and Nicolas Brunel**[e,f]

[a]Krembil Research Institute, University Health Network, Toronto, Canada; [b]Faculty of Medicine, University of Toronto, Toronto, Canada; [c]Basque Center for Applied Mathematics, Bilbao, The Basque Country, Spain; [d]Faculty of Medicine, University of the Basque Country, Leioa, Spain; [e]Department of Neurobiology, Duke University, Durham, NC, United States; [f]Department of Physics, Duke University, Durham, NC, United States

This manuscript was compiled on November 14, 2022

Persistent activity in populations of neurons, time-varying activity across a neural population, or activity-silent mechanisms carried out by hidden internal states of the neural population, have been proposed as different mechanisms of working memory (WM). Whether these mechanisms could be mutually exclusive or occur in the same neuronal circuit remain however elusive, and so do their biophysical underpinnings. While WM is traditionally regarded to depend purely on neuronal mechanisms, cortical networks also include astrocytes that can modulate neural activity. We propose and investigate a network model that includes both neurons and glia, and show that glia-synapse interactions can lead to multiple stable states of synaptic transmission. Depending on parameters, these interactions can lead in turn to distinct patterns of network activity that can serve as substrates for working memory.

neuron-glial networks | working memory | gliotransmission | spiking neuron and astrocyte models

The neural basis of working memory (WM) remains a subject of debate. A large body of evidence supports a role for sustained neural activity in prefrontal and other cortices, possibly supported by attractor dynamics in recurrently connected circuits (1). In this view, neurons hold sensory information beyond the presentation of a sensory-relevant cue by their persistent firing activity (PA). However, competing evidence suggests that WM could also be accounted for by dynamically varying activity patterns and activity-silent representations (2).

There is a growing debate on whether different mechanisms of WM could coexist within the same brain region (3), and the underpinning cellular substrate for their coexistence remains elusive (2). Activity-dependent synaptic facilitation has emerged in recent years as an appealing candidate mechanism for this coexistence (4, 5). On the one hand, it bestows cortical networks with slow time scales (from hundreds of milliseconds to minutes) that might help stabilize PA (4, 6). On the other, it can also encode memory by synaptic variables whose dynamics can sustain WM in the absence of PA (5). Although synaptic facilitation is traditionally regarded as a purely neuronal process, we consider here the possibility that it could also involve glial signaling. Among cortical glial cells, astrocytes are ubiquitous in the neuropil. They are prominently found in proximity of nerve terminals, sensing neural activity and being activated during synaptic transmission. Astrocytes can also modulate synaptic transmission by releasing transmitters – dubbed "gliotransmitters" for their glial origin – like glutamate (7). In particular, gliotransmission may promote synaptic release from excitatory terminals for several seconds, up to minutes, thus potentially contributing to WM processing, akin to short-term synaptic facilitation, but on longer time scales. In agreement with this hypothesis, astrocyte stimulation in mouse primary sensory areas increases neural firing beyond stimulation (8, 9). This phenomenon appears in association with changes of neuronal gain by higher concentrations of extracellular glutamate, possibly due to the enhanced release of this neurotransmitter by gliotransmission (8). In this fashion, gliotransmission would mediate a positive feedback on neuronal activity that could also be relevant for WM processing (6).

Results

Neuronal and synaptic correlates of working memory induced by gliotransmission. To investigate the possibility that astrocyte-mediated gliotransmission could be an active player in working memory, we started by analyzing a minimal neuron-glial circuit (Fig. 1a) of a single integrate-and-fire neuron stimulated by N synapses. A fraction f of those synapses are shared with an astrocyte, leading to interactions in both directions (Fig. 1b). Incoming action potentials (APs) trigger synaptic release (r), which occur stochastically: $r = 1$, with probability u, and 0 otherwise (Fig. 1c). We also introduce an integrate-and-fire formalism to describe astrocyte activation (v_G) in terms of slow build-up (by W per incoming AP) and fast release of intracellular calcium mediating gliotransmitter release (Materials and Methods). Since gliotransmitter release only occurs beyond some calcium threshold, and is short-lived with respect to the triggering calcium increases (Supporting Information (SI) Appendix), its timing can be approximated by the timing of intracellular calcium elevations beyond the release threshold. Specifically, we posit that when

Significance Statement

The biophysical underpinnings of working memory are of paramount interest in modern neuroscience. Working memory could be encoded by diverse patterns of neural activity, ranging from persistent firing of neuronal populations to more dynamic patterns of network activity. 'Silent' mechanisms whereby working memory is maintained by synaptic variables have also been suggested. Multiple models exist for these mechanisms but only consider neurons, ignoring glia. We propose that glia could underpin working memory, introducing models of cortical neuron-glial networks where synapse-glia signaling could account for firing and silent working memory encoding. Our theoretical arguments can explain emerging accounts of the variegated nature of working memory encoding and the possible contribution of glia to it.

M.D.P and N.B. designed the model. M.D.P. implemented the model and performed the simulations. M.D.P and N.B. did the mathematical analysis and wrote the manuscript.

The authors declare no conflict of interest, financial or otherwise.

[1]To whom correspondence should be addressed. E-mail: maurizio.depitta@uhnresearch.ca

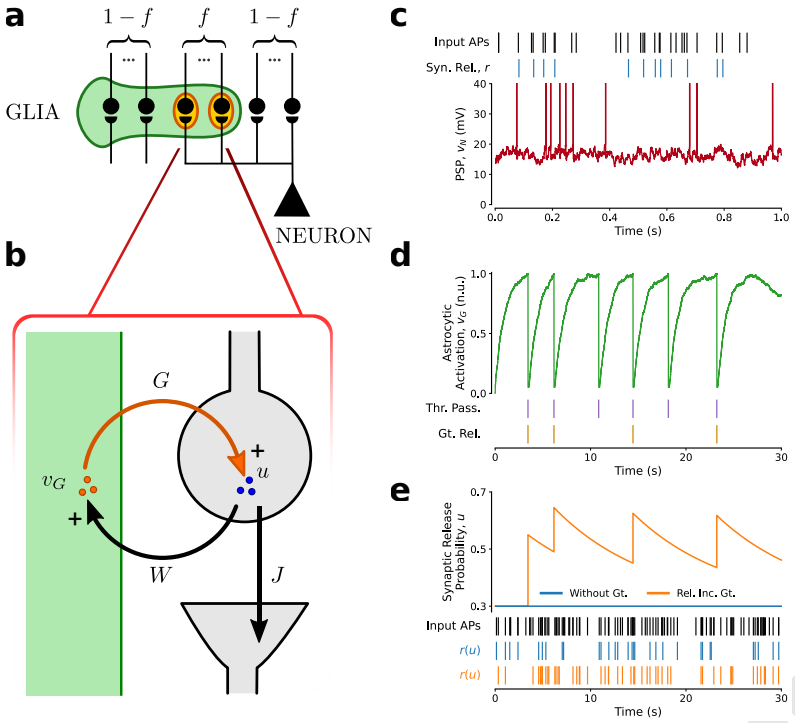

Fig. 1. Minimal neuron-glial circuit. (**a**) Schematics of a single neuron-astrocyte domain, where a fraction f of the synapses are shared by the neuron with the astrocyte. (**b**) Synapse-astrocyte positive feedback loop. Neurotransmitter release r at a presynaptic terminal, occuring with instantaneous probability u, can depolarize both the post-synaptic neuron (by an amount J), and the astrocyte (by W). Astrocyte activation can trigger glutamate release from the astrocyte which, in turn, can lead to an increase in release probability u described by a parameter G. (**c**) Incoming action potentials at a sample synapse (*black raster*) trigger stochastic neurotransmitter release (*blue raster*). The summed synaptic input from $N = 1000$ excitatory synapses drives fluctuations in the membrane potential (v_N) of a leaky integrate-and-fire neuron (*red traces*), leading to irregular firing (*vertical red bars*). (**d**) The shared synapses also stimulate the astrocyte whose activation (v_G) is equivalently described by a leaky integrate-and-fire formalism (*green trace*). Each calcium 'spike' (*purple vertical lines*) triggers stochastic glutamate (Gt.) release from the astrocyte (*yellow vertical lines*). (**e**) The instantaneous neurotransmitter release probability from a synapse modulated by astrocytic glutamate (from **d**) (*orange trace*) is shown together with the release probability from the same synapse in the absence of gliotransmission (*blue line*). *Bottom rasters* exemplify how these two scenarios results in different transmission of a train of APs (*black raster*). Parameters as in Table **??**.

$v_G = 1$, a calcium 'spike' occurs, triggering glutamate release from the astrocyte with some probability (Fig. 1d). Each gliotransmitter release event (GRE), in turn, transiently increases glutamate release probability at those synapses shared between the astrocyte and the neuron (Fig. 1e). In agreement with experimental observations (7), this increase decays slowly, with a time scale $\tau_G > 5\,\mathrm{s}$, to the value of release probability attained by the synapses in the absence of gliotransmission (SI Appendix).

In the absence of the astrocyte, this minimal circuit is memoryless - the neuronal firing rate only depends on the current inputs, and while an increase in the input rate of presynaptic APs (ν) can increase the neuron's firing rate, this rapidly goes back to baseline after the original input is restored (Fig. 2a). In the presence of gliotransmission, the neuronal response to an input can change dramatically, with two possible scenarios. In Fig. 2b, gliotransmission is triggered by stimulating the $(1-f)N$ synapses that are not shared with the neuron, while the stimulation rate of the neuron remains constant. In this fashion, gliotransmission occurs only during the stimulus presentation (*yellow marks* coinciding with the *green square pulse* in the top panels), yet it promotes a slow-decaying increase of neurotransmitter release at synapses shared between the neuron and the astrocyte (*orange trace*). This increases the net synaptic drive to the neuron, resulting in a transient increase of its firing activity that decays over time scales of the order of τ_G (*bottom raster*).

A ramping activity can be obtained when gliotransmission is triggered by synapses that also stimulate the neuron (Fig. 2c). In this case, the positive feedback of gliotransmission on synaptic stimulation can promote astrocytic glutamate release beyond the cue's presentation and, in turn, keep higher levels of synaptic release in a self-sustained manner. PA may also emerge following the cue for sufficiently strong astrocytic activation, even though presynaptic stimulation recovers to pre-cue rates. PA is generated thanks to the emergence of bistability in the rate of gliotransmitter release (ν_G), as evinced by considering the steady-state solutions for such release rate. ν_G is the inverse of the mean time between two consecutive GREs in which astrocyte activity reaches the threshold for gliotransmitter release (v_t^G) from the reset value (v_r^G) attained immediately after the first GRE. It can be expressed as a function of the time-averaged synaptic release probability $U = \langle u \rangle_{\Delta T}$ at shared synapses in a time interval $\Delta T \to \infty$ by the mean ($\mu_G(U) = fNWU\nu\tau_G$) and standard deviation of the synaptic input to the astrocyte ($\sigma_G(U) = \sqrt{W\mu_G}$), namely

$$\nu_G = \left(\tau_G^r + \int_{\frac{v_r^G - \mu_G(U)}{\sigma_G(U)}}^{\frac{v_t^G - \mu_G(U)}{\sigma_G(U)}} \mathrm{d}z \Psi_G(z) \right)^{-1} = \Phi_G\left(\mu_G(U), \sigma_G(U)\right) \quad [1]$$

where $\Psi_G(z) = \tau_G\sqrt{\pi}\exp(z^2)(1+\mathrm{erf}(z))$, and τ_G^r represents the absolute refractory period for gliotransmitter release (10, 11) (and SI Appendix). When gliotransmission does not modulate the synaptic input to the astrocyte, $\Phi_G\left(\mu_G, \sigma_G\right)$ in equation 1 provides an explicit function to estimate the average steady-state rate of gliotransmitter release at given (constant) U values. In this case, Φ_G coincides with the classic solution of the first passage-time problem of a leaky integrate-and-fire neuron with a white noise input current (11, 12). On the other hand, when the synaptic input to the astrocyte is modulated by gliotransmission, U becomes a function of ν_G (see equation **??** in the SI Appendix), and the solutions of equation 1 can be graphically found by the intersections of the straight line of slope unity with the curve given by the r.h.s. of equation 1 as a function of $U(\nu_G)$. In this scenario, besides the trivial solution for the intersection at $\nu_G \sim 0$, two other intersections may exist for $\nu_G > 0$, depending on the rate of synaptic stimulation (ν_S) of which the one at higher ν_G, is stable, while the other is not. The minimal neuron-glial circuit is thus bistable since two distinct steady-state rates of gliotransmitter release exist for the same synaptic stimulation: a very low rate when synaptic stimulation is not sufficient to promote gliotransmission, and a higher rate of a few release events per second when gliotransmission is promoted by synaptic stimulation.

Gliotransmission brings forth bistable synaptic release. Analysis of the bifurcation diagrams for $\nu_G(\nu_S)$ in Fig. 2e allows appre-

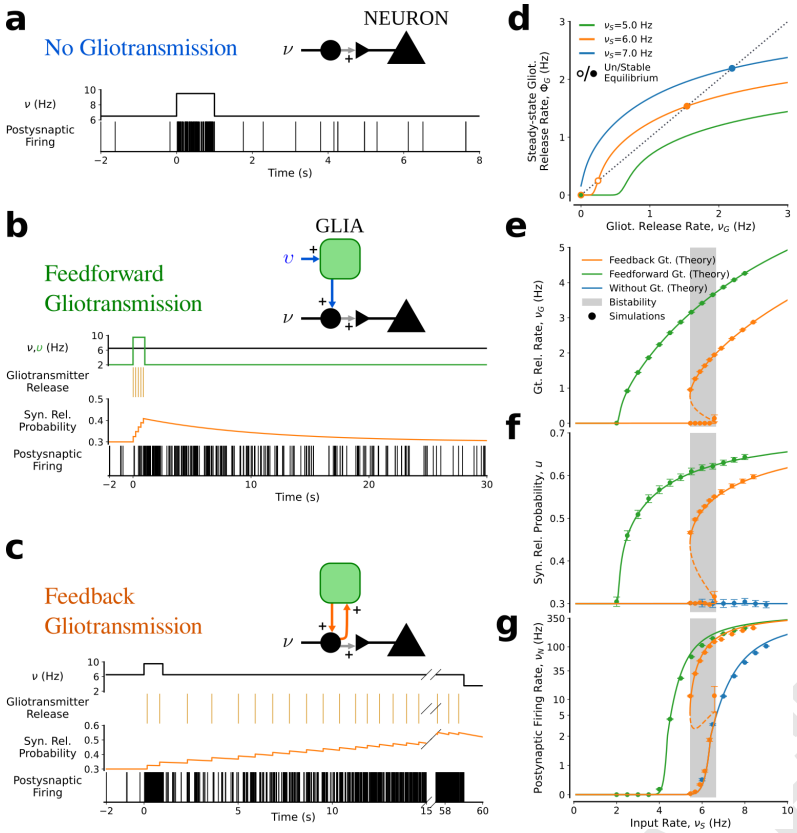

Fig. 2. Working memory in the minimal neuron-glial circuit. (**a**) In the absence of gliotransmission, the circuit is memoriless, and neuronal firing (*raster*) quickly returns to baseline right after the presentation of a square-pulse input current (*top panel*, for $0 \leq t < 1\,\mathrm{s}$). (**b**) Independent stimulation of the astrocyte (*green square pulse*), to trigger gliotransmitter release therefrom (*yellow raster*) results in the transient increase of synaptic release probability (*orange trace*) in association with a long-lasting transient increase of postsynaptic firing (*black raster*). (**c**) Postsynaptic firing can ramp up, and eventually turn persistent, when gliotransmission is stimulated by the same synapses that it modulates (*yellow raster*). When this occurs, synaptic release is bistable, leading to two stable post-synaptic firing rates, one low, the other high (*black raster*, for $t < 0$ and $t > 15\,\mathrm{s}$). (**d**-**g**) Local stability analysis of the minimal neuron-astrocyte circuit. (**d**) Graphical solutions of the steady-state rates of gliotransmitter release: one or two stable rates exist depending on the rate of synaptic stimulation (ν_S). Mapping such rates for all ν_S values provides the bifurcations diagrams for (**e**) the rate of gliotransmitter release from the astrocyte, (**f**) the synaptic release probability, and (**g**) the firing rate of the postsynaptic neuron. The sigmoid-shaped bifurcation diagrams in the presence of feedback gliotransmission hallmark the emergence of bistability with hysteresis (*orange curves* and *data points*). Theoretical curves were constructed by numerical continuation of mean-field equations (equations **??**–**??**). Data points and errorbars: mean±s.d. across 20 synapses in $n = 20$ simulations. *Solid*/*dashed curves*: stable/unstable equilibria. Parameters as in Table **??**.

ciating how bistability (*gray shaded*) only exists in the presence of positive feedback mediated by release-increasing gliotransmission on the astrocyte's synaptic input. Moreover, the sigmoid shape of the *orange diagram* associated with feedback gliotransmission reveals the existence of hysteresis, that is, the dependence of gliotransmitter release on the astrocyte's activation history. For such release to occur steadily, not only the rate of synaptic stimulation must be in the gray-shaded range, but also the astrocyte's activity must be above the *dashed line* that represents the unstable fixed point. Only in this case the increase in synaptic release ensuing from gliotransmission can promote further gliotransmitter release from the astrocyte in a self-sustained fashion that can outlast the original synaptic stimulation.

A corollary of this reasoning is that, in the presence of positive feedback by gliotransmission and for appropriate rates of synaptic stimulation, steady-state synaptic release in the minimal neuron-glial circuit may be either low, for very low gliotransmitter release, or high for sustained gliotransmitter release (Fig. 2f). These different levels of synaptic release, in turn, result in different postsynaptic firing rates (Fig. 2g). Thus, the postsynaptic neuron that would be silent or fire sporadically for low stimulation rates in the absence of gliotransmission($\nu_S < 6.5\,\mathrm{Hz}$) instead fires in the same conditions yet with sustained gliotransmitter release from the astrocyte. Hence, when an input pushes synaptic release from the low attractor to the high one, like in the simulation in Fig. 2, the neuron's activation is also expected to ramp up after the cue presentation, reminiscent of experimental observations in delay periods of delayed response tasks (3, 13, 14). The ramping-up ultimately ends with neuronal firing stabilizing at a constant steady-state rate of PA. The ensuing firing is higher than that otherwise attained by the neuron in the low synaptic release attractor, until a sufficiently long decrease in external input resets it to baseline. In this model, sustained activity can be highly irregular, with a coefficient of variation of the neuron's inter-spike interval distribution that can be higher than baseline, and also be above one (Fig. **??**), in agreement with the observed irregularity of PA in delayed response tasks (15). In addition, bistability of synaptic release and neuronal firing by feedback gliotransmission in the minimal circuit occurs robustly for a broad range of neuronal and astrocytic parameters (Fig. **??**).

Working memory in neuron-glial networks. The next question we ask is whether bistability could also emerge in large cortical neuron-glial networks. To answer this question, we considered a network of 4000 excitatory (E) and 1000 inhibitory (I) randomly connected neurons (16) that interact with 4000 astrocytes (G). Denoting $\epsilon = 1000/4000$ the E : I neuron ratio, each neuron receives exactly C_E excitatory synapses, and ϵC_E inhibitory ones from other neurons in the network. Motivated by experimental data, we consider the case where all these recurrent excitatory and inhibitory synapses stimulate astrocytes, but only excitatory ones are modulated by gliotransmission (7). In this regard, we assume that recurrent synapses can randomly connect with equal probability to any astrocyte in the network, so that each astrocyte is stimulated by K_E excitatory synapses and ϵK_E inhibitory ones (see SI Appendix). The contribution of excitatory and inhibitory synapses to neuronal depolarization is J and $-g_J J$, whereas both synapse types contribute to astrocyte activation by W (Materials and Methods).

Analysis of the asynchronous state of the ensuing EI+G network confirms the possibility of bistability by the positive feedback of gliotransmission on recurrent excitatory connections. This can be seen considering the solutions of the system of implicit equations for the network's average rates of neuronal firing (ν_N) and gliotransmitter

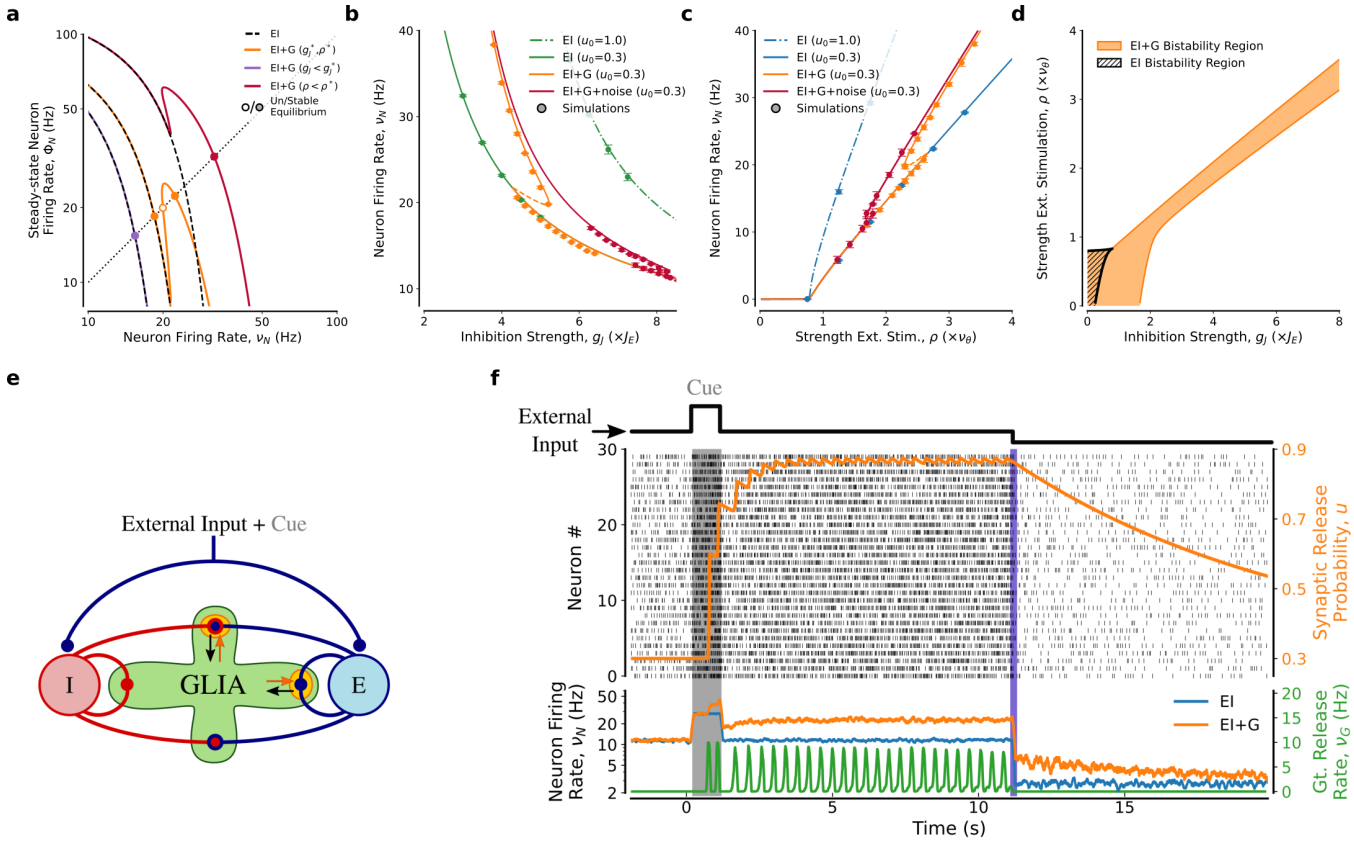

Fig. 3. Working memory in neuron-glial networks. (**a**-**d**) Bistability in a randomly-connected EI+G network. (**a**) Graphic solution of the self-consistency equations for the asynchronous state(s) (equation **??**) reveals the possibility of coexistence of two stable equilibria separated by an unstable one (*orange curve*) in a range of values of g_J and ρ ($g_J^* = 5, \rho^* = 2.2$). While stronger inhibition prevents the onset of persistent gliotransmission, resulting in low firing rates ($g_J = 6$, *purple curve*), stronger external stimuli promote gliotransmission, leading to a distinct firing rate of the asynchronous state ($\rho = 2.7$, *red curve*). Such bistability of the asynchronous state is exclusively by gliotransmission, since only one equilibrium is found solving the self-consistency equations for the mere neuronal (EI) network (*black dashed lines*), regardless of the scenario under consideration. (**b**) Firing rates in network asynchronous states as a function of recurrent inhibition, and (**c**) as a function of the external excitatory input. The *orange* bifurcation diagram for the EI+G network with basal synaptic release probability $u_0 = 0.3$, always lies between the diagrams of the EI network without gliotransmission, respectively for the same value of u_0 (*solid blue* and *green curves*), and for deterministic synaptic release ($u_0 = 1$, *dash-dotted curves*). In the case of the EI+G network there exists an intermediate range of both g_J and ρ values for two distinct asynchronous states exist: a low rate one, similar to the one that exists in the EI network in the absence of gliotransmission; and a higher rate one, resulting from ongoing, persistent gliotransmitter release from the astrocyte network. (**d**) Comparison between the bistability regions of the neuron-only EI network (*hashed area*) and the bistability region in the EI+G network (*orange area*). In the EI+G network, the bistability region is composed of two parts: (i) for $\rho < 0.8$, a region that extends bistability in EI network towards higher inhibitory drive, and (ii) for $\rho > 0.8$ a stripe that extends into the inhibition-dominated region ($g_J > 2$). This shape is a consequence of our assumption that both excitatory and inhibitory synapses stimulate astrocytes, but only excitatory ones are strengthened by gliotransmission. In this fashion, as inhibition grows, it comes to competes with release-increasing gliotransmission at excitatory connections: only when excitation reinforced by gliotransmission wins over inhibition, bistability emerges. Simulations (*circles*) agree with analytical results. Data and error bars: mean±s.d. for $n = 5$ different network realizations simulated for 20 s. (**e**-**f**) Persistent activity emerging from gliotransmission-mediated bistability in a neuron-glia network. (**e**) Random neuron-glia (EI+G) network model (Materials and Methods). (**f**) The EI+G network is stimulated by a brief square pulse (cue 'C' with rate of ∼25 Hz) for $0 \leq t < 1$ s (*dark shading*). Without gliotransmission, neuronal firing quickly returns to baseline after cue presentation (*blue trace*). In the presence of gliotransmission, the cue promotes a persistent increases of synaptic excitation (u, *top orange trace*), resulting in PA. *Black dots*: spike rasters of a representative subset of 30 excitatory neurons. The *purple bar* marks a reduction of afferent excitation, leading to a reduction in neuronal activity. Parameters as in Table **??**.

release (ν_G) (SI Appendix)

$$\nu_\alpha = \Phi_\alpha\left(\mu_\alpha(\nu_N, \nu_G), \sigma_\alpha(\nu_N, \nu_G)\right) \qquad [2]$$

where $\Phi_\alpha(\mu_\alpha, \sigma_\alpha)$ $(\alpha = N, G)$ is in the form of equation 1 and yields the firing rate of a cell in population α receiving noisy inputs of mean μ_α with standard deviation σ_α. Equations 2 generalize those for balanced neuronal networks introduced by Amit and Brunel (17) to neuron-glial networks, where the mean inputs to neurons and glia, and the corresponding amplitude of fluctuations read (SI Appendix):

$$\mu_N = C_E J\left((U - g_J\epsilon)\nu_N + \nu_X\right)\tau_N \qquad \sigma_N = \sqrt{C_E \mu_N} \qquad [3]$$

$$\mu_G = K_E W(U + \epsilon)\nu_N \tau_G \qquad \sigma_G = \sqrt{K_E \mu_G} \qquad [4]$$

In the above equations, it is convenient to express the rate of stimulation of external inputs to the network as $\nu_X = \rho\nu_\theta$ where ν_θ is the rate of stimulation needed for a neuron to fire in the absence of recurrent inputs (16). Then, as illustrated by the (*orange curve*) in Fig. 3a, two stable equilibria, reflecting UP and DOWN asynchronous states, respectively at high and low firing rates, can co-exist separated by an unstable equilibrium depending on the values of two parameters: the strength of the network's recurrent inhibitory connections (g_J), and the strength of afferent excitatory stimulation to the neurons (ρ). While bistability can exist in purely neuronal unstructured EI networks (16, 18), the presence of glia-synapse interactions dramatically expands the parameter region in which bistability occurs. A comparison of the *orange* bifurcation diagrams of the EI+G network as functions of g_J (Fig. 3) and ρ (Fig. 3c) with those of the same EI network without glia (*green* and *blue diagrams*, respectively) reveals that bistability in the EI+G network could emerge for regimes of strong

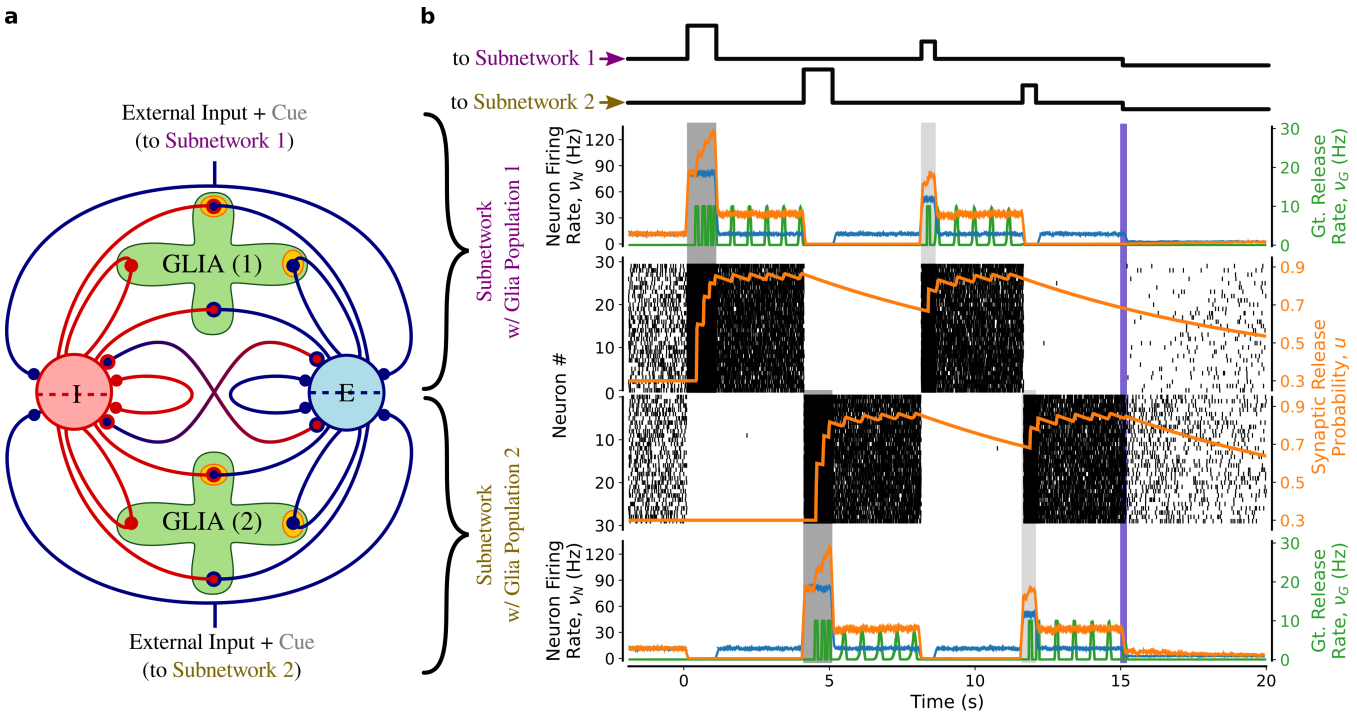

Fig. 4. Multistability in structured EI+G networks encoding two distinct memories. (**a**) Structured EI+G network model. The network of Fig. 3e is separated in two sub-networks (1 and 2) of equal E, I and G cell numbers. Recurrent synapses in each sub-network are modulated by distinct astrocyte populations (Materials and Methods). (**b**) A random subset of 50% of neurons in subnetwork 1 is stimulated by a high-frequency ($\sim$60 Hz) cue, promoting PA in subnetwork 1, while suppressing most of the subnetwork 2's activity thanks to recurrent inhibition. At $t = 4$ s, the cue is fed to the subnetwork 2, making it persistently active, while suppressing activity in subnetwork 1. Individual memories can be reactivated by weaker stimulations (30 Hz) of single subnetworks, occurring within a temporal window of about $\tau_G = 10$ s. Parameters as in Table **??**.

recurrent inhibition and strong external excitation that, in the absence of gliotransmission, could account for only one stable asynchronous state instead. Such bistability could also be found in the presence of moderate noise levels, mimicking putative gliotransmitter release ensuing from spontaneous calcium dynamics in astrocytes (19) (*red diagrams*). Moreover, it could be found for arbitrarily large values of recurrent inhibition and external excitation, in stark contrast with the mere EI network (Fig. 3d). In the latter, external excitation and recurrent inhibition exert opposite effects on the average network's firing: the former increases it, whereas the latter decreases it. In the presence of glia, however, because both excitatory and inhibitory connections promote the gliotransmitter release, these two opposite effects can compete, resulting in close but distinctly higher (respectively, lower) firing rates besides those otherwise attained by the network in the absence of gliotransmission, with strong recurrent inhibition (respectively, strong external excitation). The range for bistability in the $g_J - \rho$ plane ultimately depends on the relative scaling of the contribution of inhibitory synapses vs. excitatory ones to glial activation (Fig. **??**).

A simulation of a randomly-connected EI+G network (Fig. 3e) allows appreciating how bistability emerges in the inhibition-dominated regime by feedback gliotransmission, providing a mechanism for WM (*bottom orange trace*) in a network that would be otherwise memoryless without astrocytes (*blue trace*). Here, a short high-frequency step increase of afferent stimulation can push the network from the DOWN to the UP state, triggering PA (*bottom panel*, *orange* vs. *blue traces*). However, because the increase of excitatory drive mediated by gliotransmission competes with the strong inhibition, PA firing rates differ by just a few Hz from the DOWN state. At the same time, ongoing gliotransmission changes the internal state of excitatory synapses, providing a latent mechanism for WM by facilitation of synaptic release probability (*middle panel*, *orange trace*). This also holds for more silent versions of WM achieved by lower spontaneous activity and allows reactivating the cue's memory by weaker nonspecific inputs presented to the network, as long as gliotransmission-mediated synaptic facilitation is high enough (Figures S**??** and S**??**).

Synaptic-astrocyte connectivity can account for multi-item working memory encoding. The topology of synapse-astrocyte interactions is an additional important factor in shaping network dynamics. Different synaptic ensembles modulated by distinct astrocytes could promote discrete domains of excitation and inhibition (20), resulting in heterogeneous active neuronal populations. Consider the scenario in Fig. 4a where the astrocytes in the EI+G network belong to two disjoint populations that split the neurons into distinct subnetworks whose recurrent connections are modulated by distinct astrocytes. Without astrocytes, the selective stimulation of a subnetwork transiently promotes the firing of neurons in that subnetwork that also leads to a transient surge of feedback inhibition to the rest of the network, suppressing the firing of unstimulated neurons (*blue traces* in the *dark gray shades*), as in standard attractor neural networks with strong recurrent inhibition (21). Moreover, after cue presentation, no PA is observed as the network is dominated by inhibition. With the addition of astrocytes, the stimulated subnetwork can instead turn persistently active by the selective stimulation of the associated astrocyte population. In this way, the ensuing increase of recurrent excitation promoted by gliotrasmission remains spatially confined within the subnetwork (*top* u *orange trace*). The whole network can also be switched to another 'memory state,' by a sufficiently strong stimulation of the second subnetwork, which leads to suppression of the first (*gray shade* at $t = 4$ s). Moreover, thanks to the slow time scale τ_G of decay of the modulation of synaptic excitation by glio-

transmission, it is possible to reactivate individual memories by ∼30% weaker stimuli to individual subnetworks (*light gray shades*). In this fashion, different domains of gliotransmission from distinct astrocyte populations, promote clustered network activity. Each cluster encodes a separate WM item, and emerges as a neuronal population that is kept persistently active by spatially-segregated astrocyte activation, and the associated gliotransmission modulating synaptic release. These observations also hold for moderate noise levels of gliotransmission (Fig. **??**), mimicking spontaneous and stochastic glial activity (SI Appendix).

Discussion

The cellular and circuit bases of WM have been the subject of debate for decades. The traditional view is that WM maintenance depends on the stationary persistence of neural activity patterns representing specific memory items. However, this view has been challenged by emerging evidence that PA does not always accompany WM maintenance but could instead wax and wane as a function of the current task relevance of memoranda (13, 22). These observations spurred the idea that WM might not reside entirely in the spiking activity but could also be maintained by non-spiking, "activity-silent" mechanisms, like short-term facilitation (5). While traditionally regarded to be exclusively mediated by synaptic mechanisms, we propose that mechanisms of synaptic facilitation underpinning WM could be mediated by gliotransmission from astrocytes (23, 24).

Combining numerical simulations of biophysically realistic neuron-glial circuits with analytical calculations, we show how astrocytic gliotransmission could sustain different WM activity patterns observed experimentally, both at the level of individual neurons and large cortical networks. In our models, dynamical patterns of WM can be generated by the slowly decaying facilitation of synaptic weights by gliotransmission – up to tens of seconds slower than the decay of traditional short-term synaptic facilitation (7) – and can encompass ramping-up, persistent, and ramping-down neuronal firing patterns. These patterns could occur network-wide or be confined to portions of the network under the influence of specific astrocyte populations, suggesting that cortical networks could exploit distinct astrocyte populations to encode multiple WM items.

Multi-item WM is not a prerogative of neuron-glial networks. It can be generated by purely neuronal networks in which connectivity has been structured by Hebbian plasticity, both with static synapses (25), and dynamic synapses (5). Here, we propose a scenario in which synaptic connectivity is left unstructured but in which distinct ensembles of potentiated synapses encoding distinct memoranda emerge through different domains of gliotransmitter-mediated synaptic facilitation under the influence of different astrocyte populations.

In our network model consisting of two astrocyte populations, triggering PA in the subnetwork associated with one astrocyte population suppresses memory-related firing in the remainder of the network under the influence of the other astrocyte population. However, in the portion of the network where activity is suppressed, a "silent" memory encoding persists, thanks to the slowly-vanishing synaptic facilitation mediated by gliotransmission. Presenting a noisy input to the silent subnetwork before the decay of gliotransmission-mediated facilitation can indeed restore PA in that subnetwork while switching WM encoding in the active subnetwork to activity-silent. This behavior supports recent accounts that activity-based vs. activity-silent forms of memory maintenance, which have traditionally been regarded as mutually exclusive, could rather coexist in the same brain region (3). We suggest that heterogeneous domains of gliotransmission ensuing from different astrocyte populations (26, 27) could be the biophysical substrate for the coexistence of such different WM forms.

Opto- and chemo-genetic approaches adopted to study astrocytes' influence on other memory forms could be used to monitor and manipulate the molecular pathways underpinning gliotransmission selectively and test our hypotheses (28, 29). In this regard, optogenetics imaging of astrocytic calcium activity in WM tasks supports our simulations revealing the temporally-precise delayed onset of the astrocyte's activity with neuronal firing at WM onset, maintenance, and recall (30). Likewise, genetic suppression of synaptically-activated astrocytic calcium signaling correlates with reduced cognitive performance in classic WM experiments like the Y-maze-based spontaneous alternation task (31), and the T-maze-based delayed nonmatching-to-place task (23). While other mechanisms of astrocytic origin rather than gliotransmission could underpin such experimental observations, compelling evidence exists that agrees with our model predictions insofar as WM encoding could originate from gliotransmission-mediated modulations of the network's excitatory vs. inhibitory balance (23).

It will be important to characterize better experimentally the anatomy of the connections between cortical synapses, and astrocytes (32), given our observation that multistability could emerge from neuron-glia networks in which astrocytes define specific neuronal clusters. Clustered neuronal activity could emerge from the heterogeneous astrocyte arrangement across the brain (27), within brain regions and in specific circuits (33). Such a scenario is in agreement with recent experimental and theoretical studies that identifies the anatomy of individual astrocytes (34, 35), as well as their possible arrangement into syncytial networks (36, 37), as key aspects in the emergence of neuronal firing ensembles in cognitive-related tasks (32).

On the other hand, the same astrocyte population could also dynamically exert multiple neuromodulatory actions on distinct neurons by a combination of different calcium-dependent pathways (38, 39) and synaptic activity requirements (40, 41). This aligns with the growing recognition that sensory input dynamics could dictate the spatial extent and temporal dynamics of astrocytic calcium signals (39, 40, 42), and thus, potentially, of gliotransmission (7, 32, 43). In turn, modeling arguments suggest this as a biophysical substrate to relay information of multiple memoranda by minimally-overlapping spatial domains of calcium-dependent gliotransmission (44). It remains however unclear to what extent the number of possible memoranda that could be stored by neuron-glial networks depends on the reciprocal arrangement of astrocytes with respect to neurons and synaptic elements (44).

The modulations of intrasynaptic calcium by extrasynaptically-located presynaptic receptors bound by gliotransmitters could exert varied effects on synaptic transmission besides increasing the release probability. For instance, they could interfere with mechanisms of short-term plasticity, speeding up the refilling process of synaptic vesicles (45) thus enabling sustained release at the synaptic terminals for extended periods, as required by our theory (e.g., Fig. 3f). At the same time, independent theoretical investigations suggest that the modulation of short-term plasticity by gliotransmission, in combination with the network's noise, could also stabilize (or not) WM depending on the ongoing activity, ultimately controlling WM duration by modulating its mechanisms of onset and termination (46). Thus, including short-term synaptic plasticity in our neuron-glial models is expected to enrich the activity requirements for different WM forms emerging by gliotransmission.

We focus here on the well-documented homosynaptic scenario of regulation of synaptic release by gliotransmission, where the same synapses that stimulate an astrocyte are also modulated by gliotrans-

mission from it. Nonetheless, we predict our theory to also hold for gliotransmitter-mediated increases of postsynaptic efficacy and heterosynaptic modes of gliotransmission (7), as long as they mediate a positive feedback loop in the circuit that can be self-sustained. On the other hand, gliotransmission could also nonlinearly depend on the history of activation of interacting astrocytic domains (41, 47), which could respectively be accounted for by nonlinear extensions of the integrate-and-fire astrocyte model, and the addition of astrocyte-astrocyte interactions in the EI+G network model.

While we have restricted ourselves to multistability between several asynchronous states, other, more dynamic scenarios for WM maintenance could also be dependent on gliotransmission. Dynamical regulations of neuronal gain could alter cortical tuning properties of neuronal ensembles with possible repercussions on dynamic WM encoding (13, 22, 48). There is also emerging evidence that astrocytic gliotransmission could modulate cognitive-relevant brain rhythms (9, 40, 49) which might play a role in WM maintenance (50, 51). These intriguing possibilities require future efforts to characterize the variety of possible neuron-glial networks' spatio-temporal dynamics.

Materials and Methods

Single neuron-astrocyte domain. We consider a minimal neuron-glial circuit of a neuron (N) and an astrocyte (G). The neuron has $N = 1000$ identical synapses in total feeding into the circuit, that are independently stimulated by trains of Poisson-distributed action potentials (APs), modelled by Dirac delta functions, i.e., $s_i(t) = \sum_k \delta(t - t_i^k)$ for the i-th synapse. A fraction f of these synapses is "shared" by the neuron and the astrocyte. Those synapses stimulate both cells, and are modulated by gliotransmission from the astrocyte. The remaining $(1 - f)N$ synapses stimulate instead only the astrocyte, in the scenario of feedforward gliotransmission (Fig. 2b), or only the neuron, in the case of feedback gliotransmission (Fig. 2c).

Glutamate release from synaptic terminals is described by a Bernoulli process: when an AP reaches a presynaptic terminal, release occurs with probability u, with each release occurring independently from all other ones. We thus define a train of synaptic releases $\tilde{s}_i(t) = \sum_k r_i^k \delta(t - t_i^k)$, where r_i^k are independent Bernoulli random variables describing release occurring with probability $u(t_i^k)$ following the k-th spike at synapse i. Each glutamate release instantaneously depolarizes the neuron by J, while increasing astrocytic activation by W. Neuronal depolarization (v_N) is described by a leaky integrate-and-fire (LIF) formalism, such that

$$\frac{dv_N}{dt} = -\frac{v_N}{\tau_N} + J \sum_j \tilde{s}_j(t) \qquad [5]$$

where τ_N is the characteristic decay time constant for neuronal depolarization. Every time v_N reaches a threshold value v_t^N, the neuron generates an AP, v_N is reset to v_r^N, and subsequently held to this value for a refractory period τ_r^N. We also consider a LIF description for astrocytic activation. This activation can be thought as being an increasing function of the astrocyte's intracellular Ca^{2+} concentration, which critically regulates gliotransmitter release (SI Appendix). Astrocytic Ca^{2+} activity (v_G) is driven by synaptic stimulation $i_G(t)$ according to

$$\frac{dv_G}{dt} = -\frac{v_G}{\tau_G} + i_G(t) \qquad [6]$$

with $i_G(t) = W \sum_j \tilde{s}_j(t)$, and τ_G is a lumped time constant for stimulus integration by astrocytic Ca^{2+} signaling (Supplementary Text Section **??**). Because gliotransmitter release only occurs when Ca^{2+} reaches a threshold v_t^G, a gliotransmitter release event (GRE) is set to occur when $v_G > v_t^G$, following which v_G is reset to and held at baseline v_r^G for a refractory period τ_r^G (SI Appendix).

Both astrocytic calcium signaling (42) and gliotransmitter release have a stochastic component (52, 53), therefore we also consider a stochastic description of GREs. That is, GREs are modelled by i.i.d. Bernoulli random variables r_G^k whose value is 1 (release success) with probability u_G, and 0 (release failure) otherwise, for each astrocytic threshold crossing k. The single gliotransmitter release event in this context represents the 'total release' of gliotransmitter per threshold crossing, and it does not account for potentially different mechanisms of gliotransmitter release (19). In this fashion, the sequence of GREs originating from the astrocyte, each occurring at instants t_G^k, is described by $g(t) = \sum_k r_G^k \delta(t - t_G^k)$.

At synapses that are shared with the astrocyte, synaptic release probability u is taken to be modulated by GREs from the astrocyte according to (Supplementary Text Section **??**)

$$\frac{du}{dt} = \frac{u_0 - u}{\tau_p} + G(\xi - u)g(t) \qquad [7]$$

where u_0 stands for the (baseline) synaptic release probability in the absence of gliotransmission; G and $\xi > u_0$ control the strength of the positive feedback of gliotransmission on synaptic release, and τ_p is the decay time constant of the increase of synaptic release mediated by gliotransmission.

Neuron-glial network. The model network of excitatory and inhibitory neurons originally introduced by Brunel (16) is extended to include astrocytes. The resulting neuron-glial network is composed of $N_G = 4000$ astrocytes (G), together with $N_E = 4000$ excitatory neurons (E) and $N_I = 1000$ inhibitory neurons (I). All neurons (astrocytes) are described by a LIF formalism, with identical membrane time constants τ_N (τ_G), and firing thresholds v_t^N (v_t^G). Neurons in the network are randomly connected such that each neuron receives $C_E = 400$ connections from excitatory neurons, and $C_I = 100$ connections from inhibitory neurons. Additionally, all neurons are supposed to be stimulated by C_E excitatory afferents from the same cell population (X) outside the network. Synaptic release from neuron j to i (r_{ij}) is probabilistic at recurrent excitatory connections, with a probability (u_{ij}) that depends on GREs from the astrocytes, as described above. For simplicity, we consider identical postsynaptic potential amplitudes $J > 0$ at excitatory synapses, and $-g_J J$ at inhibitory synapses. The external synapses are taken to be stimulated by independent Poisson processes with rate $\nu_X = \rho\nu_\theta$, where $\nu_\theta = v_t^N/(JC_E\tau_N)$ is the external frequency that leads to an average membrane potential equal to the neuronal firing threshold. In this fashion, the external input to the network is modelled by a background noisy current, with mean $\mu_X = C_E J \nu_X \tau_N$ and variance $\sigma_X^2 = J\mu_X$. Denoting by $\tilde{s}_{ij}(t) = \sum_k r_{ij}^k \delta(t - t_j^k)$ the train of synaptic releases from excitatory neuron j, where r_{ij}^k are independent Bernoulli r.v. with release probability $u_{ij}(t_j^k)$, and by $s_j^I(t)$ the spike train for inhibitory neuron j, the depolarization v_i^α of the i-th neuron in population $\alpha = E, I$ evolves according to:

$$\frac{dv_i^\alpha}{dt} = -\frac{v_i^\alpha}{\tau_N} + J \sum_{j \in \mathcal{E}_i} \tilde{s}_{ij}(t) - g_J J \sum_{j \in \mathcal{I}_i} s_j^I(t) + \frac{\mu_X}{\tau_N} + \frac{\sigma_X}{\tau_N}\eta_X(t) \qquad [8]$$

where $\eta_X(t)$ is a temporally uncorrelated normal random variable with mean 0 and variance 1, and $\mathcal{E}_i$ (respectively, $\mathcal{I}_i$) denotes the set of all excitatory (respectively, inhibitory) synapses impinging onto neuron i.

All synapses, regardless of their type, can depolarize glial cells. This reflects the experimental observation, that both glutamatergic (excitatory), and GABAergic (inhibitory) synapses can trigger calcium-dependent gliotransmission (7, 54). We assume that all synapses contribute equally to astrocytic depolarization by W. Moreover, given that the molecular machinery for gliotransmission is found in juxtaposition with synaptic terminals (55), we assume that each excitatory synapse stimulating an astrocyte, is also modulated by gliotransmission from the latter. Although gliotransmission has also been documented at inhibitory synapses, we limit our analysis to pathways of release-increasing gliotransmission to excitatory synapses only, as the latter accounts for the majority of available evidence supporting gliotransmission (43).

Accordingly, the depolarization v_G^i of the i-th astrocyte and the release probabilities of excitatory synapses are described by the set of coupled differential equations

$$\frac{dv_i^G}{dt} = -\frac{v_i^G}{\tau_G} + W \sum_{(j,l) \in \mathcal{A}_i^E} \tilde{s}_{jl}(t) + W \sum_{(j,l) \in \mathcal{A}_i^I} s_l^I(t) \qquad [9]$$

$$\frac{du_{jl}}{dt} = \frac{u_0 - u_{jl}}{\tau_p} + G(\xi - u_{jl})g_i(t) \qquad \text{for all } (j,l) \in \mathcal{A}_i^E \qquad [10]$$

where g_i is the train of GREs originating from the k-th astrocyte, and $\mathcal{A}_i^\alpha$ is the set of all α synapses impinging on astrocyte i. Specifically, we consider different scenarios for connections between recurrent synapses and astrocytes. In the random network of Figures 3e,f, each astrocyte picks a random subset $\mathcal{N}_s/N_G$ of synapses, out of a total of $\mathcal{N}_s = (C_E + C_I)(N_E + N_I)$ recurrent

synapses. In the EI+G network of Fig. 4 instead, the EI neuron network was partitioned into two subnetworks of equal numbers of neurons ($(N_E+N_I)/2$) and synapses ($\mathcal{N}_s/2$). Then, recurrent connections of those subnetwork were assigned to distinct populations of $N_G/2$ astrocytes.

In our neuron-glial networks, the number of neurons per astrocyte is 1.25, and an astrocyte domain can contain between 300 and 600 synapses, depending on whether we consider two distinct astrocyte populations, or one population only (Fig. 4). These figures agree with experimental data (56) in mice, and are also in line with whole-brain estimations of the neuron-to-glia ratio by isotropic fractionation (SI Appendix). Likewise, the fact that only recurrent synapses ($\mathcal{N}_s$ in total), but not external ones ($C_E(N_E + N_I)$ in total) are coupled with astrocytes in our networks accounts for approximately 55% of synapses associated with astrocytes, reflecting recent data suggesting that 40–80% of cortical synapses are likely astrocyte-regulated (57, 58).

Mathematical analysis. Mean-field analyses of the minimal neuron-glial circuit (Fig. 2) and the unstructured EI+G network (Fig. 3) were performed along the lines of Amit and Brunel (17). We choose the network's parameters such that the mean firing rate of excitatory neurons equals that of inhibitory cells, $\nu_E = \nu_I = \nu_N$. Both ν_N. Details can be found in the Supplementary Text Section **??**.

Numerical methods. Simulations and mean field analysis used custom code implemented in C/C++, Python 3.x, and the Python-based Brian 2.x simulator (59). Numerical integration used either an event-based scheme, or the Euler-Maruyama method with time step $dt = 10\,\mu s$. Bifurcation diagrams were generated by Matcont 6.x in Matlab® (R2017a, MathWorks) (60). Simulations were performed on an Intel® Xeon® 12-core CPU E5-1660 @3.30 GHz Linux desktop. The Python classes to reproduce the neuron-glial circuits of this study are available from the authors upon request.

ACKNOWLEDGMENTS. We thank Paolo Bonifazi and Yair Lakretz for comments on the manuscript, and Marcel Stimberg for technical support on the code to simulate the spiking models. This work was originally funded by a Marie Skłodowksa-Curie International Outgoing Fellowship to MDP (Project 331486 "Neuron-Astro-Nets").

1. C Constantinidis, et al., Persistent spiking activity underlies working memory. *J. Neurosci.* **38**, 7020–7028 (2018).
2. J Kamiński, U Rutishauser, Between persistently active and activity-silent frameworks: novel vistas on the cellular basis of working memory. *Annals New York Acad. Sci.* **1464**, 64–75 (2020).
3. J Barbosa, et al., Interplay between persistent activity and activity-silent dynamics in the prefrontal cortex underlies serial biases in working memory. *Nat. Neurosci.* **23**, 1016–1024 (2020).
4. O Barak, M Tsodyks, Working models of working memory. *Curr. opinion neurobiology* **25**, 20–24 (2014).
5. M Mongillo, O Barak, M Tsodyks, Synaptic theory of working memory. *Science* **319**, 1543–1546 (2008).
6. R Chaudhuri, I Fiete, Computational principles of memory. *Nat. Neurosci.* **19**, 394–403 (2016).
7. A Araque, et al., Gliotransmitters travel in time and space. *Neuron* **81**, 728–739 (2014).
8. G Perea, A Yang, ES Boyden, M Sur, Optogenetic astrocyte activation modulates response selectivity of visual cortex neurons in vivo. *Nat. communications* **5**, 3262 (2014).
9. KE Poskanzer, R Yuste, Astrocytes regulate cortical state switching in vivo. *Proc. Natl. Acad. Sci.* **113**, E2675–E2684 (2016).
10. DJ Amit, M Tsodyks, Quantitative study of attractor neural network retrieving at low spike rates. I. Substrate-spikes, rates and neuronal gain. *Network: Comput. Neural Syst.* **2**, 259 (1991).
11. AJ Siegert, On the first passage time probability problem. *Phys. Rev.* **81**, 617 (1951).
12. LM Ricciardi, *Diffusion processes and related topics in Biology*. (Springer Science & Business Media) Vol. 14, (1977).
13. MG Stokes, 'activity-silent'working memory in prefrontal cortex: a dynamic coding framework. *Trends Cogn. Sci.* **19**, 394–405 (2015).
14. HK Inagaki, L Fontolan, S Romani, K Svoboda, Discrete attractor dynamics underlies persistent activity in the frontal cortex. *Nature* **566**, 212–217 (2019).
15. A Compte, et al., Temporally irregular mnemonic persistent activity in prefrontal neurons of monkeys during a delayed response task. *J. Neurophysiol.* **90**, 3441–3454 (2003).
16. N Brunel, Dynamics of sparsely connected networks of excitatory and inhibitory spiking neurons. *J. Comput. Neurosci.* **8**, 183–208 (2000).
17. D Amit, N Brunel, Model of global spontaneous activity and local structured activity during delay periods in the cerebral cortex. *Cereb. Cortex* **7**, 237–252 (1997).
18. EM Tartaglia, N Brunel, Bistability and up/down state alternations in inhibition-dominated randomly connected networks of lif neurons. *Sci. reports* **7**, 1–14 (2017).
19. I Savtchouk, A Volterra, Gliotransmission: Beyond black-and-white. *J. Neurosci.* **38**, 14–25 (2018).
20. MM Halassa, T Fellin, H Takano, JH Dong, PG Haydon, Synaptic islands defined by the territory of a single astrocyte. *J. Neurosci.* **27**, 6473–6477 (2007).
21. N Brunel, XJ Wang, Effects of neuromodulation in a cortical network model of object working memory dominated by recurrent inhibition. *J. Comput. Neurosci.* **11**, 63–85 (2001).
22. M Lundqvist, P Herman, EK Miller, Working memory: Delay activity, yes! Persistent activity? Maybe not. *J. neuroscience* **38**, 7013–7019 (2018).
23. S Mederos, et al., Gabaergic signaling to astrocytes in the prefrontal cortex sustains goal-directed behaviors. *Nat. Neurosci.* **24**, 82–92 (2021).
24. G Perea, A Araque, Astrocytes potentiate transmitter release at single hippocampal synapses. *Science* **317**, 1083–1086 (2007).
25. DJ Amit, A Bernacchia, V Yakovlev, Multiple-object working memory—a model for behavioral performance. *Cereb. Cortex* **13**, 435–443 (2003).
26. OA Bayraktar, et al., Astrocyte layers in the mammalian cerebral cortex revealed by a single-cell in situ transcriptomic map. *Nat. Neurosci.* **23**, 500–509 (2020).
27. D Lanjakornsiripan, et al., Layer-specific morphological and molecular differences in neocortical astrocytes and their dependence on neuronal layers. *Nat. Commun.* **9**, 1–15 (2018).
28. BS Khakh, MV Sofroniew, Diversity of astrocyte functions and phenotypes in neural circuits. *Nat. Neurosci.* **18**, 942 (2015).
29. A Kol, I Goshen, The memory orchestra: the role of astrocytes and oligodendrocytes in parallel to neurons. *Curr. Opin. Neurobiol.* **67**, 131–137 (2021).
30. Z Lin, et al., Entrainment of astrocytic and neuronal Ca^{2+} population dynamics during information processing of working memory in mice. *Neurosci. Bull.* pp. 1–15 (2021).
31. J Nagai, et al., Specific and behaviorally consequential astrocyte Gq GPCR signaling attenuation in vivo with iβARK. *Neuron* **109**, 2256–2274 (2021).
32. M Santello, N Toni, A Volterra, Astrocyte function from information processing to cognition and cognitive impairment. *Nat. Neurosci.* **22**, 154–166 (2019).
33. R Refaeli, et al., Features of hippocampal astrocytic domains and their spatial relation to excitatory and inhibitory neurons. *Glia* **69**, 2378–2390 (2021).
34. LP Savtchenko, DA Rusakov, Regulation of rhythm genesis by volume-limited, astroglia-like signals in neural networks. *Philos. Transactions Royal Soc. B: Biol. Sci.* **369**, 20130614 (2014).
35. J Schummers, H Yu, M Sur, Tuned responses of astrocytes and their influence on hemodynamic signals in the visual cortex. *Sci. STKE* **320**, 1638 (2008).
36. C Giaume, CC Naus, JC Sáez, L Leybaert, Glial connexins and pannexins in the healthy and diseased brain. *Physiol. Rev.* **101**, 93–145 (2021).
37. G Dallérac, J Zapata, N Rouach, Versatile control of synaptic circuits by astrocytes: where, when and how? *Nat. Rev. Neurosci.* **19**, 729–743 (2018).
38. TV Vaidyanathan, M Collard, S Yokoyama, ME Reitman, KE Poskanzer, Cortical astrocytes independently regulate sleep depth and duration via separate gpcr pathways. *Elife* **10**, e63329 (2021).
39. R Martín, R Bajo-Grañeras, R Moratalla, G Perea, A Araque, Circuit-specific signaling in astrocyte-neuron networks in basal ganglia pathways. *Science* **349**, 730–734 (2015).
40. G Perea, et al., Activity-dependent switch of GABAergic inhibition into glutamatergic excitation in astrocyte-neuron networks. *Elife* **5**, e20362 (2016).
41. A Covelo, A Araque, Neuronal activity determines distinct gliotransmitter release from a single astrocyte. *eLife* **7**, e32237 (2018).
42. A Semyanov, C Henneberger, A Agarwal, Making sense of astrocytic calcium signals – from acquisition to interpretation. *Nat. Rev. Neurosci.* **21**, 551–564 (2020).
43. M De Pittà, N Brunel, A Volterra, Astrocytes: orchestrating synaptic plasticity? *Neuroscience* (2015).
44. SY Gordleeva, et al., Modelling working memory in spiking neuron network accompanied by astrocytes. *Front. Cell. Neurosci.* **15**, 86 (2021).
45. JS Dittman, AC Kreitzer, WG Regehr, Interplay between facilitation, depression, and residual calcium at three presynaptic terminals. *J. Neurosci.* **20**, 1374–1385 (2000).
46. S Becker, A Nold, T Tchumatchenko, Formation and synaptic control of active transient working memory representations. *BioRxiv* (2020).
47. T Pirttimaki, S Hall, H Parri, Sustained neuronal activity generated by glial plasticity. *J. Neurosci.* **31**, 7637–7647 (2011).
48. KK Sreenivasan, M D'Esposito, The what, where and how of delay activity. *Nat. Rev. Neurosci.* **20**, 466–481 (2019).
49. HS Lee, et al., Astrocytes contribute to gamma oscillations and recognition memory. *Proc. Nat. Acad. Sci. USA* p. E3343–E3352 (2014).
50. EK Miller, M Lundqvist, AM Bastos, Working memory 2.0. *Neuron* **100**, 463–475 (2018).
51. M Lundqvist, et al., Gamma and beta bursts underlie working memory. *Neuron* **90**, 152–164 (2016).
52. M Potokar, et al., Astrocytic vesicle mobility in health and disease. *Int. J. Mol. Sci.* **14**, 11238–11258 (2013).
53. DN Bowser, BS Khakh, Two forms of single-vesicle astrocyte exocytosis imaged with total internal reflection fluorescence microscopy. *Proc. Natl. Acad. Sci. USA* **104**, 4212–4217 (2007).
54. G Losi, L Mariotti, G Carmignoto, GABAergic interneuron to astrocyte signalling: a neglected form of cell communication in the brain. *Philos. Transactions Royal Soc. B: Biol. Sci.* **369**, 20130609 (2014).
55. P Jourdain, et al., Glutamate exocytosis from astrocytes controls synaptic strength. *Nat. Neurosci.* **10**, 331–339 (2007).
56. H Chai, et al., Neural circuit-specialized astrocytes: transcriptomic, proteomic, morphological, and functional evidence. *Neuron* **95**, 531–549 (2017).
57. L Abdeladim, et al., Multicolor multiscale brain imaging with chromatic multiphoton serial microscopy. *Nat. Commun.* **10**, 1–14 (2019).
58. N Kasthuri, et al., Saturated reconstruction of a volume of neocortex. *Cell* **162**, 648–661 (2015).
59. M Stimberg, R Brette, DF Goodman, Brian 2, an intuitive and efficient neural simulator. *Elife* **8**, e47314 (2019).
60. A Dhooge, W Govaerts, YA Kuznetsov, HGE Meijer, B Sautois, New features of the software matcont for bifurcation analysis of dynamical systems. *Math. Comput. Model. Dyn. Syst.* **14**, 147–175 (2008).

PNAS
www.pnas.org

Supplementary Information for

Multiple forms of working memory emerge from synapse-astrocyte interactions in a neuron-glia network model

Maurizio De Pittà and Nicolas Brunel

Corresponding author: Maurizio De Pittà. E-mail: maurizio.depitta@uhnresearch.ca

This PDF file includes:

Supporting Information Text

1. Biological background

A. Biophysical justification of the leaky integrate-and-fire astrocyte model. The leaky integrate-and-fire approximation of the astrocyte (LIFA) introduced in this study is based on experimental observations of astrocytic calcium (Ca^{2+}) signaling and Ca^{2+}-dependent exocytosis of common gliotransmitters like glutamate and ATP. Possible extensions of the LIFA to model other gliotransmission pathways are briefly addressed at the end.

Integration. The Ca^{2+} signal responsible for gliotransmitter release builds up in an integrative fashion (1, 2), with the number of stimuli delivered to the astrocyte (e.g. by optogenetic Ca^{2+} uncaging, or by electrical stimulation of synaptic afferent) (3, 4), the duration of stimulation (3), and its strength (see Supplementary Figure 10 in 5, 6).

Leakage. Multiple cell-intrinsic mechanisms for Ca^{2+} homeostasis are present in astrocytes that recover baseline intracellular Ca^{2+} levels and resemble Ca^{2+} leakage from the astrocyte cytosol (7). These mechanisms range from subcellular buffering in combination with diffusion away from the Ca^{2+} source (8–10), to transmembrane fluxes by ion exchangers (11, 12). Although these mechanisms are generally nonlinear, the minimal stimulation of putative gliotransmitter-competent astrocytic domains – the equivalent of the domain's impulse response to quantal synaptic release – displays a Ca^{2+} signal that decays exponentially (1, 13).

Firing. Astrocytic Ca^{2+} elevations triggered by physiological synaptic stimulation appear with a latency of a few hundreds of milliseconds to a second from the onset of stimulation (14–16), and are generally characterized by an early, quasi-linear phase, followed by a rapid increase to peak (1, 5, 17). At the same time, Ca^{2+}-dependent gliotransmitter release is a threshold phenomenon that requires intracellular Ca^{2+} to reach a threshold concentration to promote gliotransmitter exocytosis (18, 19).

Reset and refractoriness. Release of glutamate from astrocytes prominently occurs during the rising phase of a Ca^{2+} transient (18, 20), but stops when Ca^{2+} plateaus or decreases (20). Additional sources of refractoriness could also be accounted for by the Ca^{2+} pathways underpinning astrocytic glutamate release. A well-studied pathway in this context is that of Ca^{2+} release from the ER (21, 22), whose timing depends on the gating kinetics of second-messenger-activated Ca^{2+} channels on the ER membrane (23). In parallel, other molecular mechanisms can contribute to the recovery of baseline Ca^{2+} concentrations. These include: Ca^{2+}-dependent enzymes related to second-messenger pathways underpinning astrocytic Ca^{2+} signaling (24, 25); active uptake by Ca^{2+}-ATPases on the plasma and the endoplasmic reticulum membranes (12, 26), uptake by mitochondria (27), and intracellular buffering (9, 10).

Beyond gliotransmitter exocytosis. The leaky integrate-and-fire description could, in principle, be adopted to also account for Ca^{2+}-dependent mechanisms of gliotransmitter release other than exocytosis, like glutamate and GABA release by bestrophin-1 channels (28–30), GABA release by reversed transporters (31, 32), or gliotransmitter release by hemichannels (33, 34). Moreover, it could also be taken as a first-order approximation of other Ca^{2+}-independent, astrocytic endocrine pathways that show some degree of stimulus-integration and threshold dynamics: e.g., ROS-dependent glutamate release by volume-sensitive channels (35), lactate release by acute glycogenolysis (36, 37), or glutamine release by sustained synaptic release (38). Aside from the consideration that some of these release routes have been linked to pathology (21), the properties of routes of transmitter release not mediated by exocytosis, are expected to produce extracellular transmitter concentrations that are different, over time, from those ensuing from exocytosis, possibly with different functional consequences (39) that call for additional modeling (40).

B. Derivation of the gliotransmission model. Synaptic release probability u depends on intracellular Ca^{2+} at synaptic terminals (41). The arrival of an action potential at a synapse opens Ca^{2+}-permeable channels, triggering a rapid increase of intrasynaptic Ca^{2+} promoting neurotransmitter release. Besides action potentials, however, several other mechanisms, including gliotransmission (42), can modify intrasynaptic Ca^{2+} thereby modulating synaptic release probability u. Gliotransmitters can indeed target receptors that are usually located extrasynaptically on presynaptic terminals. Despite their variegated nature, their dependence on the type of gliotransmitter released from perisynaptic astrocytic processes, and possibly on a combination of functional and anatomical constraints (43), all these receptors can nonetheless be linked with the regulation of intrasynaptic Ca^{2+}, and thus of synaptic release (44, 45). The underpinning molecular details are not fully understood, but they are not necessary if we make the hypothesis that u is a smooth function of the fraction γ of receptors activated by gliotransmission through intrasynaptic Ca^{2+}around the baseline value of synaptic release probability u_0, in the absence of gliotransmission (i.e., for $\gamma = 0$). Then, we can use a Taylor expansion of u up to first order,

$$u(\gamma) \simeq u_0 + \left.\frac{du}{d\gamma}\right|_{\gamma=0} \gamma + O\left(\gamma^2\right). \quad [1]$$

The first-order term in the above equation can be written as $du/d\gamma(\gamma = 0) = \xi - u_0$, where $0 \leq \xi \leq 1$ accounts for the nature of gliotransmission on synaptic release – release-decreasing for $\xi < u_0$, and release-increasing for $\xi > u_0$ (46). Assuming that the onset of the effect of receptor's activation on synaptic release is much faster than its decay time (τ_p), the fraction of receptors bound by gliotransmitter release events $g(t)$ (occurring at instants t_G^k), i.e. $g(t) = \sum_k \delta(t - t_G^k)$, evolves according to (46)

$$\tau_p \frac{d\gamma}{dt} = -\gamma + G(1-\gamma)g(t)\tau_p \quad [2]$$

where G accounts for the gliotransmission's efficiency, and can be thought as the equivalent strength of the astrocyte-to-synapse connection mediated by gliotransmission. Finally, differentiating both sides of equation 1 using 2 provides

$$\tau_p \frac{du}{dt} = u_0 - u + G(\xi - u)g(t)\tau_p. \quad [3]$$

2. Mean field analysis

A. Single neuron-astrocyte domain (SGD) model.

A.1. Self-consistent equations for mean firing rates. We start with the SGD model described by equations 5–7 in the main text with fN shared synapses, and $(1-f)N$ non-shared synapses. We consider a regime in which both neuron and astrocyte receive a large number of synaptic inputs per integration time τ_α ($\alpha = N, G$). Each input makes a small contribution compared to the cell's firing threshold, i.e., $J \ll v_t^N$, $W \ll v_t^G$, and can be approximated by a Poisson process where a Dirac delta function describes each incoming action potential. In this scenario, the synaptic current to the neuron (respectively, astrocyte) can be approximated by the sum of a temporal average part plus a fluctuating Gaussian white noise, i.e.

$$i_\alpha = \mu_\alpha + \sigma_\alpha \sqrt{\tau_\alpha}\eta_\alpha(t) \quad [4]$$

with $\langle \eta_\alpha \rangle = 0$ and $\langle \eta_\alpha(t)\eta_\alpha(t') \rangle = \delta(t-t')$. Therefore, the equation for the depolarization of the neuron (respectively, astrocyte), coincide with that of an Ornstein-Uhlenbeck (OU) process (e.g. 47)

$$\tau_\alpha \frac{dv_\alpha}{dt} = -v_\alpha + \mu_\alpha + \sigma_\alpha \sqrt{\tau_\alpha}\eta_\alpha(t). \quad [5]$$

In the above equation, the average μ_α is related to the cell's firing rate ν_α and is a sum of shared (s) and non-shared inputs (n), i.e. $\mu_\alpha = \mu_{\alpha,s} + \mu_{\alpha,n}$. Hence, it follows from equations 5 and 6 that

$$\mu_{N,s} = fNJU\nu_S\tau_N \qquad \mu_{G,s} = fNWU\nu_S\tau_G \quad [6]$$

$$\mu_{N,n} = (1-f)NJu_0\nu_S\tau_N \qquad \mu_{G,n} = (1-f)NWu_0\nu_S\tau_G \quad [7]$$

where $U = \langle u \rangle_{\Delta T}$ denotes the time-averaged synaptic release probability at shared synapses over a time window $\Delta T \to \infty$, i.e.,

$$U = \frac{u_0 + \xi G \nu_G \tau_p}{1 + G\nu_G\tau_p} \quad [8]$$

and we absorbed u_G in G for simplicity of notation.

The fluctuating part in equation 4 is given by the fluctuations in the sum of shared and non-shared Poisson inputs incoming at rate ν_S, i.e. $\sigma_\alpha^2 = \sigma_{\alpha,s}^2 + \sigma_{\alpha,n}^2$. Its magnitude, then, is given by

$$\sigma_{N,s}^2 = fNJ^2U\nu_S\tau_N \qquad \sigma_{G,s}^2 = fNW^2U\nu_S\tau_G \quad [9]$$

$$\sigma_{N,n}^2 = (1-f)NJ^2u_0\nu_S\tau_N \qquad \sigma_{G,n}^2 = (1-f)NW^2u_0\nu_S\tau_G \quad [10]$$

Finally, the output spike rate of the neuron (respectively, astrocyte) is given by the inverse of the mean time between two consecutive events in which each cell's depolarization reaches threshold plus the absolute refractory period, i.e.

$$\nu_\alpha = \Phi_\alpha(\mu_\alpha, \sigma_\alpha) \quad [11]$$

where Φ can be analytically derived solving the mean first-passage time problem of the OU process in equation 5 (47–50), i.e.,

$$\Phi_\alpha(\mu_\alpha, \sigma_\alpha) = \left(\tau_\alpha^r + \int_{y_r^\alpha}^{y_t^\alpha} \mathrm{d}z \Psi_\alpha(z) \right)^{-1} \quad [12]$$

with

$$\Psi_\alpha(z) = \tau_\alpha \sqrt{\pi} \exp(z^2)(1 + \mathrm{erf}(z)) \quad [13]$$

$$y_r^\alpha = (v_r^\alpha - \mu_\alpha)/\sigma_\alpha \quad [14]$$

$$y_t^\alpha = (v_t^\alpha - \mu_\alpha)/\sigma_\alpha \quad [15]$$

The set of equations 6–11 provides a set of self-consistent equations for the gliotransmission rate, leveraging the fact that $U = U(\nu_G)$. In particular, because gliotransmission influences the firing of the postsynaptic neuron by modulation of presynaptic release but not vice versa, the steady-state of the SGD model must only satisfy the equation

$$\nu_G = \Phi_G\left(\mu_G(U(\nu_G)), \sigma_G(U(\nu_G))\right) \quad [16]$$

whose solutions can be solved graphically (Fig. 2a).

A.2. Local stability analysis. To analyze the stability of the states described by the self-consistent equations 6–11, we adopt a heuristic approach. We approximate the dynamics of the firing rates of both neuron (ν_N) and astrocyte (ν_G) by linear ODEs with time constants τ_N and τ_G respectively, and whose fixed points ν_N^*, ν_G^* solve equation 11. Note that this approximation is exact only in the low firing rate limit (51). Accordingly, defining $\bar{\theta} = \min(\tau_N, \tau_G, \tau_p)$, $\theta_\alpha = \tau_\alpha/\bar{\theta}$ ($\alpha = N, G, p$), and $\theta = t/\bar{\theta}$ the normalized time, we thus approximate the dynamics around the stationary states of the system as

$$\theta_N \frac{d\nu_N}{d\theta} = -\nu_N + \Phi_N(\mu_N, \sigma_N) \quad [17]$$

$$\theta_G \frac{d\nu_G}{d\theta} = -\nu_G + \Phi_G(\mu_G, \sigma_G) \quad [18]$$

$$\theta_p \frac{d\upsilon}{d\theta} = -\upsilon + U(\nu_G) \quad [19]$$

where we introduced the variable υ ('upsilon') to denote the temporal mean of $\langle u \rangle_{\delta T}$ over a fast time scale, i.e. $\tau_N, \tau_G < \delta T \ll \tau_p$. When $\tau_N \ll \tau_G,\ \tau_p$ (see Section Model parameters), neuronal dynamics can be assumed to be at steady state with respect to astrocytic dynamics, so that the slow dynamics of the SGD model can be approximated by

$$\theta_G \frac{d\nu_G}{d\theta} = -\nu_G + \Phi_G(\mu_G(\upsilon), \sigma_G(\upsilon)) \quad [20]$$

$$\theta_p \frac{d\upsilon}{d\theta} = -\upsilon + U(\nu_G) \quad [21]$$

The stability of the fixed points ν_N^*, ν_G^*, U^* of equations 17–19 is determined by the Jacobian of this reduced system:

$$\mathbf{M} = \begin{pmatrix} -\theta_G^{-1} & \theta_G^{-1}\partial_\upsilon \Phi_G \\ \theta_p^{-1}\partial_G U & -\theta_p^{-1} \end{pmatrix} \quad [22]$$

whose determinant is given

$$\det \mathbf{M} = (\theta_G \theta_p)^{-1}(1 - \partial_\upsilon \Phi_G \partial_G U) \quad [23]$$

where $\partial_\upsilon \equiv \partial/\partial\upsilon$, $\partial_G \equiv \partial/\partial\nu_G$ are evaluated at $(\nu_G, \upsilon) = (\nu_G^*, U^*)$. Since $\mathbf{M}$ has a negative trace, the stability condition for the fixed points boils down to $\det \mathbf{M} > 0$. Hence, the condition for local stability of gliotransmission is given by the inequality

$$\partial_\upsilon \Phi_G \partial_G U < 1 \quad [24]$$

In the above equation, $\partial_\upsilon \Phi$ is always positive, so the instabilities can only arise if $\partial_G U$ is positive, i.e. in the case of release-increasing gliotransmission ($\xi > u_0$). In this case, bistability of synaptic release emerges through a saddle-node bifurcation (Figures 2b–d). In practice, the condition for bistability requires that $\partial_\upsilon \Phi = (\partial_G U)^{-1}$ at the bifurcation point $(\nu_G, \upsilon) = (\breve{\nu}_G, \breve{U})$, that is (by equation 12)

$$(X_G \partial_\upsilon \mu_G + Y_G \partial_\upsilon \sigma_G)|_{(\breve{\nu}_G, \breve{U})} = \left. \frac{(1 + G\tau_p \nu_G)^2}{(\xi - u_0) G \tau_p} \right|_{(\breve{\nu}_G, \breve{U})} \quad [25]$$

where

$$X_G = \partial_\mu \Phi_G = \frac{\Phi_G^2}{\sigma}(\Psi_G(y_t^G) - \Psi_G(y_r^G)) \quad [26]$$

$$Y_G = \partial_\sigma \Phi_G = \frac{\Phi_G^2}{\sigma}(y_t^G \Psi_G(y_t^G) - y_r^G \Psi_G(y_r^G)) \quad [27]$$

$$\partial_\upsilon \mu_G = fNW\nu_S\tau_G \quad [28]$$

$$\partial_\upsilon \sigma_G = \partial_\upsilon\left(\sqrt{W\mu_G}\right) = \frac{1}{2}\sqrt{\frac{W}{\mu_G}}\partial_\upsilon \mu_G. \quad [29]$$

B. Coefficient of variation of the inter-spike interval distribution. The squared coefficient of variation (CV) of postsynaptic inter-spike intervals can be analytically derived in terms of moments of the first-passage time (T_N) distribution of the OU process given by equation 5, and reads

$$\mathrm{CV}^2 = \frac{\mathrm{var}(T_N)}{\langle T_N \rangle^2} = \frac{\langle T_N^2 \rangle - \langle T_N \rangle^2}{\langle T_N \rangle^2} \quad [30]$$

where (52)

$$\langle T_N \rangle = \frac{1}{\nu_N} \quad [31]$$

$$\langle T_N^2 \rangle = \frac{1}{\nu_N^2} + \frac{2\sqrt{\pi}}{\tau_N} \int_{y_r^N}^{y_t^N} \mathrm{d}u\, e^{u^2} \int_{-\infty}^{u} \mathrm{d}z \Psi_N(z)(1 + \mathrm{erf}(z)) \quad [32]$$

so that

$$\mathrm{CV}^2 = \frac{2\sqrt{\pi}}{\tau_N}\nu_N^2 \int_{y_r^N}^{y_t^N} \mathrm{d}u\, e^{u^2} \int_{-\infty}^{u} \mathrm{d}z \Psi_N(z) \quad [33]$$

Hence, it suffices to know the mean firing rate of the postsynaptic neuron to estimate the CV of the corresponding inter-spike interval distribution.

In general, when the mean input is sub-threshold, i.e., $\mu_N < v_t^N$, spike discharge is triggered by fluctuations in the input current, and firing is irregular with CV values close to one or above. For mean inputs above the firing threshold instead, that is when $\mu_N > v_t^N$, spike discharges are more regular, and the CV decreases to zero. How sharply the neuron transitions from firing irregularly to regularly (or vice versa) depends on the amplitude of the fluctuations of the input current, that is, the noise level σ_N. In the absence of gliotransmission, with a neuron membrane time constant $\tau_N = 20\,\mathrm{ms}$, large values of σ_N resulting in CV > 1 can be achieved for low presynaptic rates (ν_S) when the neuron's after-spike reset potential approaches the firing threshold (53). In this scenario, equation 33 describes a CV vs. ν_S curve that is non-monotonic with a maximum value at $\mu_N(\nu_S) < v_r^N$ (see Fig. S1a,c, *blue* and *cyan curves*). Intuitively, this is possible because the proximity of the reset potential to the firing threshold allows for small input noise to be sufficient to trigger neuronal firing. At the same time, the after-spike reset mechanism promotes noise fluctuations further, ultimately accounting for short inter-spike intervals with higher probability. Inclusion of gliotransmission does not change this mechanism (Fig. S1), but may account for CV > 1 at lower presynaptic rates thanks to the increase of synaptic release, and thus of the average mean postsynaptic depolarization (equation 6).

C. Neuron-glial network (EIG) model.

C.1. Self-consistent equations for mean rates. Derivation of the mean-field equations for the EIG network follows analogous assumptions on connection weights used in the SGD case. We posit that $N_I = \epsilon N_E$, whereby it follows that $C_I = \epsilon C_E$. We denote by $K_\alpha = (C_E + C_I)N_\alpha/N_G$ $(\alpha = E, I)$ the total number of excitatory (respectively inhibitory) synapses per astrocyte. Moreover, we take the weights of connections from inhibitory synapses to astrocytes to be proportional to those from excitatory synapses, i.e., $W_{ijk}^{\alpha I} = g_W W$ $(g_W > 0)$. Finally, we consider the case in which all external afferents to the network are stimulated by Poisson-distributed spike trains incoming at equal rate ν_X. With this regard, we express the rate of external stimulation as $\nu_X^N = \rho\nu_\theta^N$, where $\nu_\theta^N = v_t^N/(C_E J_E \tau_N)$ represents the external frequency needed for the mean external input to reach a neuron's firing threshold in the absence of recurrent input (52). In a similar fashion, we define a threshold rate for spontaneous astrocytic activation by $\nu_\theta^G = v_t^G/(KW\tau_G)$, where $K = K_E + K_I$ is the average number of synapses impinging on an astrocyte; and we express the rate of spontaneous astrocyte activation by $\nu_X^G = \rho_G \nu_\theta^G$. Accordingly, we proceed to distinguish between recurrent (l) and external (x) components of the mean and fluctuating (noisy) parts of synaptic currents in neurons (N) and astrocytes (G), for which it is

$$\mu_N = \mu_{N,l} + \mu_{N,x} \quad [34]$$
$$\mu_{N,l} = C_E J(U - g_J\epsilon)\nu_N\tau_N \quad [35]$$
$$\mu_{N,x} = C_E J\rho\nu_\theta\tau_N \quad [36]$$

$$\mu_G = \mu_{G,l} \quad [37]$$
$$\mu_{G,l} = K_E W(U + g_W\epsilon)\nu_N\tau_G \quad [38]$$
$$\mu_{G,x} = KW\rho_G\nu_\theta^G\tau_G \quad [39]$$

$$\sigma_N^2 = \sigma_{N,l}^2 + \sigma_{N,x}^2 \quad [40]$$
$$\sigma_{N,l}^2 = C_E J^2(U + g_J^2\epsilon)\nu_N\tau_N \quad [41]$$
$$\sigma_{N,x}^2 = C_E J^2\rho\nu_\theta\tau_N \quad [42]$$

$$\sigma_G^2 = \sigma_{G,l}^2 + \sigma_{G,x}^2 \quad [43]$$
$$\sigma_{G,l}^2 = K_E W^2(U + g_W^2\epsilon)\nu_N\tau_G \quad [44]$$
$$\sigma_{G,x}^2 = KW^2\rho_G\nu_\theta^G\tau_G. \quad [45]$$

Putting in relief the functional dependence on the two firing rates ν_N, ν_G, and noting that $U = U(\nu_G)$ (equation 8), we can express ν_G as a function F of ν_N, i.e.,

$$\nu_G = \Phi_G(\mu_G(\nu_N, \nu_G), \sigma_G(\nu_N, \nu_G)) \Rightarrow \nu_G = F(\nu_N). \quad [46]$$

In turn, the latter can be replaced in the equation of ν_N, thereby obtaining the self-consistent equation

$$\nu_N = \Phi_N\big(\mu_N(\nu_N, \nu_N), \sigma_G(\nu_N, \nu_N)\big) = \Phi_N\big(\mu_N(\nu_N, F(\nu_N)), \sigma_G(\nu_N, F(\nu_N))\big). \quad [47]$$

which can conveniently be solved graphically (Fig. S3a).

C.2. Local stability analysis. To analyze the stability of the stationary (asynchronous) states of the EIG network, we use the same heuristic approach as in section A.2. As in the SGD model, we define a normalized time $\vartheta = t/\bar{\vartheta}$ with $\bar{\vartheta} = \min(\tau_N, \tau_G, \tau_p)$, and express the time constants as $\vartheta_\alpha = \tau_\alpha/\bar{\vartheta}$. The dynamics around the asynchronous states of the EIG network are approximated by the following system of ODEs

$$\vartheta_N \frac{d\nu_N}{d\vartheta} = -\nu_N + \Phi_N(\mu_N(\nu_N, \upsilon), \sigma_N(\nu_N, \upsilon)) \quad [48]$$

$$\vartheta_G \frac{d\nu_G}{d\vartheta} = -\nu_G + \Phi_G(\mu_G(\nu_N, \upsilon), \sigma_G(\nu_N, \upsilon)) \quad [49]$$

$$\vartheta_p \frac{d\upsilon}{d\vartheta} = -\upsilon + U(\nu_G) \quad [50]$$

where $\upsilon = \langle u \rangle_{\delta T}$ with $\tau_\alpha < \delta T \ll \tau_p$. We define the diagonal matrix $\mathbf{\Theta} = \mathrm{diag}(\vartheta_N, \vartheta_G, \vartheta_p)$. The Jacobian matrix of the system described by equations 48–50 is

$$\mathbf{M} = \mathbf{\Theta}^{-1} \begin{pmatrix} -1 + \partial_N \Phi_N & 0 & \partial_\upsilon \Phi_N \\ \partial_N \Phi_G & -1 & \partial_\upsilon \Phi_G \\ 0 & \partial_G U & -1 \end{pmatrix} \quad [51]$$

where $\partial_N \equiv \partial/\partial\nu_N$, $\partial_G \equiv \partial/\partial\nu_G$, $\partial_\upsilon \equiv \partial/\partial\upsilon$ are evaluated at the fixed point $(\nu_N, \nu_G, \upsilon) = (\nu_N^*, \nu_G^*, U^*)$. The analytical expression of $\partial_G U$ is given by equation 25, whereas the other partial derivatives read

$$\partial_\beta \Phi_\alpha = X_\alpha \partial_\beta \mu_\alpha + Y_\alpha \partial_\beta \sigma_\alpha \qquad (\alpha, \beta = N, G, u) \quad [52]$$

$$X_\alpha = \partial_\mu \Phi_\alpha = \frac{\Phi_\alpha^2}{\sigma_\alpha} (\Psi_\alpha(y_\theta^\alpha) - \Psi_\alpha(y_r^\alpha)) \quad [53]$$

$$Y_\alpha = \partial_\sigma \Phi_\alpha = \frac{\Phi_\alpha^2}{\sigma_\alpha} (y_\theta^\alpha \Psi_\alpha(y_\theta^\alpha) - y_r^\alpha \Psi_\alpha(y_r^\alpha)). \quad [54]$$

The eigenvalues of the Jacobian matrix of the EIG system are solved numerically (Figures S3b,c). It is however informative to consider the determinant of this matrix, i.e.

$$\det \mathbf{M} = (\vartheta_N \vartheta_G \vartheta_p)^{-1} \left(-1 + \partial_N \Phi_N + \partial_G U (\partial_N \Phi_G \partial_u \Phi_N + (1 - \partial_N \Phi_N) \partial_u \Phi_G)\right). \quad [55]$$

Bistability of the network asynchronous states emerge through a saddle-node bifurcation, at which $\det \mathbf{M} = 0$. In the right hand side of equation 55, we can distinguish two terms:

- A purely neuronal term, $-1 + \partial_N \Phi_N$. This terms coincides with the determinant of the EI network in the simplified ('model A') framework. In particular the network is stable when $\partial_N \Phi_N < 1$ (54).

- An astrocyte-dependent term, $\Lambda = \partial_G U (\partial_N \Phi_G \partial_u \Phi_N + (1 - \partial_N \Phi_N) \partial_u \Phi_G)$. This term affects the condition for stability of the EI network, which becomes $\partial_N \Phi_N < 1 - \Lambda$. If the EI network is originally stable without gliotransmission, then it is straightforward to see that instabilities may only arise for $\Lambda > 0$, i.e. release-increasing gliotransmission, since $\partial_G U > 0$.

3. Model parameters

A. Estimation of glial parameters.

Network size parameters. The majority of available data on Ca^{2+}-dependent gliotransmission currently comes from experiments on protoplasmic astrocytes of the grey matter in rodents; thus, we constrain our following estimations to the murine brain. The ratio of non-neuronal cells (comprising glial and endothelial cells) to neurons in the brain of mice and rats is estimated in the range of 0.88–1.34 (Supplementary Table 2 in 55). Excluding endothelial cells from these figures, we can thus predict lower values for the true glial-to-neuron ratio (GNR) (56). In our simulations, we set $N_G = N_E$, with $N_E = 4000$, $N_I = 1000$, $\epsilon = N_I/N_E = 0.25$, corresponding to a GNR $= N_G/(N_E + N_I) = 0.8$. On the other hand, if we regard the "astrocytes" in our models more like "astrocytic domains" that are competent for gliotransmission, rather than individual cells, then the GNR is little informative (57). From this perspective, a justification of the number of astrocytic domains in our simulations could be based on considering that such domains possibly co-localize with astrocytic branching processes that account for >75% of the cell volume (5). Based on the only available observation that domain-like putative gliotransmission-competent Ca^{2+}-spikes could roughly account for 10–15% of individual process volumes (5), and considering an average of 3–10 primary processes per cortical astrocyte (5, 58, 59), we end up with an estimation of 0.75–3.75% of the astrocytic volume per Ca^{2+} microdomain. For cortical astrocytes, whose volumes appear to be variegated across different cortical layers and be comprised between $5.5 \cdot 10^4$–$8.1 \cdot 10^4 \mu m^3$ (60), this means domain volumes in the range of ∼410–2850 μm^3. With an average density of 0.8–1 synapses/μm^3 (61, 62), we get an estimate of ∼320–2850 synapses per astrocytic domain. In this study, we consider networks with a number of synapses per astrocyte generally between >310 (Figures 4) and $K_E + K_I = 625$ synapses/astrocyte (Figures 3 and 4).

Astrocyte activation. The decay time of Ca^{2+} spikes triggering gliotransmitter release can be considerably fast, with an original estimation in cultures of $\tau_G = 0.4$–0.6 s (18), although recent estimates hint τ_G values as low as <30–250 ms (13). A complication is that τ_G seems dependent on the local process geometry, with larger τ_G values associated with larger domains (13). We estimate instead the absolute refractory

period τ_G^r, considering the maximum possible rate of GREs. Because gliotransmitter release correlates with the rising phase of a Ca^{2+} spike (18, 20), in the presence of consecutive spikes, the maximum GRE rate must be comprised between the full-width half-maximum of a Ca^{2+} spike and their period, whose minima are estimated in the ranges of <0.2–1.5 s (Supplementary Figure 5 in 5) and ∼0.2–0.7 s, respectively (18, 63). These figures for τ_G and τ_G^r can be considerably larger when considering somatic Ca^{2+} events (40). Finally, regarding the LIFA threshold and reset potential, since these quantities are introduced by our modeling argument, without loss of generality, we consider a normalized scale for the (equivalent) depolarization of the astrocyte such that baseline astrocytic activity (in the absence of noise) is 0. In contrast, the threshold for gliotransmitter release is $v_t^G = 1$, and v_r^G is arbitrarily set in this range.

Gliotransmission. Recent estimates of time scales of synaptic neurotransmitter release by gliotransmitters provide decay times τ_p in the range of ∼5–100 s and rise times of <0.05–30 s (40). Although the rise time depends on the protocol of stimulation of gliotransmission, in general, much shorter rise times than decay times are observed for sensory-triggered gliotransmission in vivo (64–66), which support our modeling assumption of instantaneous onset of synaptic modulation after gliotransmitter release. The remainder of parameters of gliotransmission – u_G, G, ξ – are instead arbitrarily set since, to the best of our knowledge, there exist no experimental data that would allow us to constrain their values.

Synaptic transmission. Release probability (u_0) at cortical synapses is generally low and suggested to be in the range of 0.1–0.5 (67). In our simulations we only consider the case of probabilistic excitatory synapses ($u_{0,E} = 0.3$) and deterministic inhibitory synapses ($u_{0,I} = 1$). We leave to future investigations the scenario in which inhibitory synaptic transmission would be probabilistic (67, 68) and regulated by astrocytic gliotransmission (69–72).

B. Simulation-specific parameter sets. Model parameters used in the simulations of the SGD and the EIG models are summarized in Tables S1 and S2 respectively, except for the cases listed below.

- Fig. 1: **c** $\nu_S = 30\,\mathrm{Hz}$, $J = 0.12\,\mathrm{mV}$; **d** $\nu_S = 5\,\mathrm{Hz}$, $G = 0.68$, $u_G = 0.55$; **e** $\nu_S = 4\,\mathrm{Hz}$, $G = 0.72$, $u_G = 0.55$.
- Fig. 3: **f** high-frequency cue for $\rho = 3.5$; reduced baseline activity for $\rho = 1$.
- Fig. 4: **b** high-frequency cues for $\rho = 5.5$; read-out stimuli for $\rho = 3.0$.

Table S1. Parameter values used in the simulations of the SGD model.

Symbol	Description	Value	Units
	Neuron dynamics		
v_r^N	Reset potential	19	mV
v_t^N	Firing threshold	20	mV
τ_N	Membrane time constant	20	ms
τ_N^r	Absolute refractory period	2	ms
	Astrocyte dynamics		
v_r^G	Equivalent reset potential	0.2	–
v_t^G	Equivalent firing threshold	1.0	–
τ_G	Ca^{2+} time constant	0.5	s
τ_G^r	Absolute refractory period	0.1	s
	Synaptic transmission		
u_0	Resting release probability (exc. synapses)	0.3	–
f	Fraction of shared synapses	0.5	–
J	Excitatory PSP (on neurons)	0.4	mV
W	Equivalent Excitatory PSP (on astrocytes)	$1.8{\cdot}10^{-3}$	–
	Gliotransmission		
u_G	Gliotransmitter release probability	1.0	–
G	Strength of gliotransmission	0.05	–
ξ	Polarity of gliotransmission	0.8	–
τ_p	Decay time constant	10	s

Table S2. Parameter values used in the simulations of the EIG network model.

Symbol	Description	Value	Units
	Neuronal dynamics		
v_r^N	Reset potential	10	mV
v_t^N	Firing threshold	20	mV
τ_N	Membrane time constant	20	ms
τ_N^r	Absolute refractory period	2	ms
	Astrocytic dynamics		
v_r^G	Equivalent reset potential	1	–
v_t^G	Equivalent firing threshold	0.2	–
τ_G	Ca^{2+} time constant	0.5	s
τ_G^r	Absolute refractory period	0.1	s
	Synaptic connections		
$u_{0,E}$	Resting release probability (exc. synapses)	0.3	–
$u_{0,I}$	Resting release probability (inh. synapses)	1	–
J	Excitatory PSP (on neurons)	0.2	mV
g_J	Scaling of synaptic inhibition	5.5	–
W	Equivalent excitatory PSP (on astrocytes)	$3.2{\cdot}10^{-4}$	–
g_W	Scaling of inhibition to astrocytes	1.0	–
	External stimulation		
ρ	Baseline external stimulation (neurons) ($\times\nu_\theta^N$)	2.0	–
ρ_G	Baseline external stimulation (astrocytes) ($\times\nu_\theta^G$)	$0.0^\dagger$	–
	Gliotransmission		
u_G	Gliotransmitter release probability	1.0	–
G	Strength of gliotransmission	0.5	–
ξ	Polarity of gliotransmission	0.8	–
τ_p	Decay time constant	10	s

† External noise input to astrocytes is only taken into account in the simulations in the Supplementary Figures S5 and S6.

Supplementary Figures

Fig. S1. Coefficient of variation (CV) of the postsynaptic inter-spike-interval distribution in the minimal neuron-glial circuit. When neuronal parameters allow for postsynaptic firing with CV>1 (53), release-increasing gliotransmission can dramatically change the range of presynaptic activity rates (ν_S) to record such CV values. (**a**) Considering shared synapses stimulating both the neuron and the astrocyte ($f > 0$) accounts for different CV>1 values for the same level of presynaptic activity. Consistently with the scenario of bistability illustrated in Figs. 2a-d, at low levels of presynaptic activity and for not too strong inputs to the astrocyte ($f = 0.5$, *red curve* and *data*), the higher CV value is associated with ongoing gliotransmission, while the lower coincides with the value attained in the absence thereof. On the other hand, stronger inputs to the astrocyte ($f = 0.8$, *orange curve* and *data*), can quickly make CV values in the presence of gliotransmission decrease below those observed in the absence of gliotransmission. Larger fractions of shared synapses can indeed promote high rates of gliotransmitter release, resulting in robust increases of synaptic release, which, in turn, can depolarize the postsynaptic neuron beyond the spiking threshold more regularly (i.e., CV<1). (**b**) How much gliotransmission increases synaptic release is another factor that can modulate CV values. For example, as we increase the effect parameter ξ beyond the occlusion scenario ($\xi = u_0$, *blue curve*), the emergence of bistability accounts for CV>1 values that are larger in the presence of gliotransmission than without it. The range of presynaptic rates for which this phenomenon can be observed generally grows with $\xi > u_0$ (compare *purple* and *orange curves*), as far as the gliotransmitter-mediated increase of synaptic drive to the neuron is not too strong to promote neuronal firing with some degree of irregularity (i.e., CV>1). (**c**) Besides parameters related to the nature of neuron-glial coupling, like f or ξ, the nature of synaptic connections in terms of their neurotransmitter release probability is a further factor modulating the effect of gliotransmission on the CV. Specifically, at fixed connectivity ($f = 0.8$), CV>1 can be attained for broader ranges of presynaptic rates when synaptic release probability is low to moderate (i.e. $u_0 < 0.5$, *orange* vs. *curves*). CV curves were computed based on equation 33. Data points and error bars represents mean±s.m.e. over $100 \leq n \leq 1000$ simulations. Other parameters as in Table S1.

Fig. S2. Ranges of bistability in the minimal neuron-glial circuit model as a function of the rate of afferent stimulation (ν_S) and the different neuronal and glial parameters. Regions with analogous shapes are colored alike. *Solid rose lines* mark the parameters values from Table S1, also adopted to compute the bifurcation diagrams of Fig. 2.

Fig. S3. Regions for bistability in the EI+G network for different scaling of the inhibitory synapses (W_I) vs. excitatory ones (W_E) impinging on the astrocytes (Section Self-consistent equations for mean rates). (**a**) The case $W_I = W_E$ considered in all simulations of this study is reproduced from Fig. 3d for the sake of comparison with different scaling considered in the other panels. In this case, the competition between inhibition and excitation enhanced by gliotransmission account for bistability at arbitrarily high values of both, drawing a characteristic strip that spans across the plane ρ vs. g_J. (**b**) The width of such strip and its slope, roughly quantifiable by the ratio ρ/g_J for points in it, inversely correlates with $k = W_I/W_E$. We illustrate this concept, considering in this panel the case where $W_I = 2W_E$. In comparison with **a**, it may be noted how the range of bistability, quantified by the height (width) of the strip for fixed values of g_J (respectively, ρ), decreases. In this case in fact, smaller increases of external stimulation are required to promote robust increases of inhibition with respect to **a**, reducing the bistability range. This is further illustrated in (**c**) where we consider the possibility that W_I scales like J_I with respect to excitatory connections, that is $W_I = g_J W_E$. This makes the growth of inhibition with gliotransmission strongly nonlinear (as a result that g_J enters in both equations of ν_G and ν_N (rather than only in the latter as in the previous cases). This ultimately results in bistability disappearing for growing g_J and ρ values. Parameters as in Table S2.

Fig. S4. Activity-silent WM by gliotransmission. A high-frequency cue ($\rho = 3$) is delivered to all neurons in the network at $t = 0$ (*dark shading*). The cue triggers gliotransmission that, in turn, promotes synaptic release (u) at excitatory connections. After the cue however, neural activity increases little (< 5 Hz) with respect to before the cue's presentation (~ 2 Hz), and slowly recovers to baseline. In this fashion, the synaptic variable u encodes the memory of the cue. This memory can be retrieved and refreshed by weak read-out signals ($\rho = 2$, *light shadings*) delivered to the whole network, as far as u attains values not too far from those right after the cue. Baseline external stimulation was fixed at $\rho = 1$. Other network parameters as in Table S2.

Fig. S5. Effect of glial noise. The same network of Fig. S4 is considered with the addition of a noisy external input to glia. The latter promotes sustained gliotransmitter release with respect to the scenario without glial noise (*middle panel*, *red* vs. *green traces*, respectively), resulting in the emergence of persistent firing at low rates (*bottom panel*, *red trace*). In this fashion, synaptic release at excitatory connections (u, *red trace* in the *top panel*) is persistently high, and the memory can be retrieved at any instant as far as the external input to the background is not reduced (*purple bar*) beyond a critical value that cannot guarantee astrocyte activation. Simulation parameters as in Fig. S4 except for $\rho_G = 0.5$.

Fig. S6. Robustness of clustered neuron-glial network activity in the presence of glial noise. The same network of Fig. 4 is considered in the presence of a noisy external input to the astrocytes. The network can still encode for multiple memories, by subnetworks associated with individual glial populations, as far as glial (G) noise levels are moderate. Simulation parameters as in Fig. 4 except for $\rho_G = 0.5$.

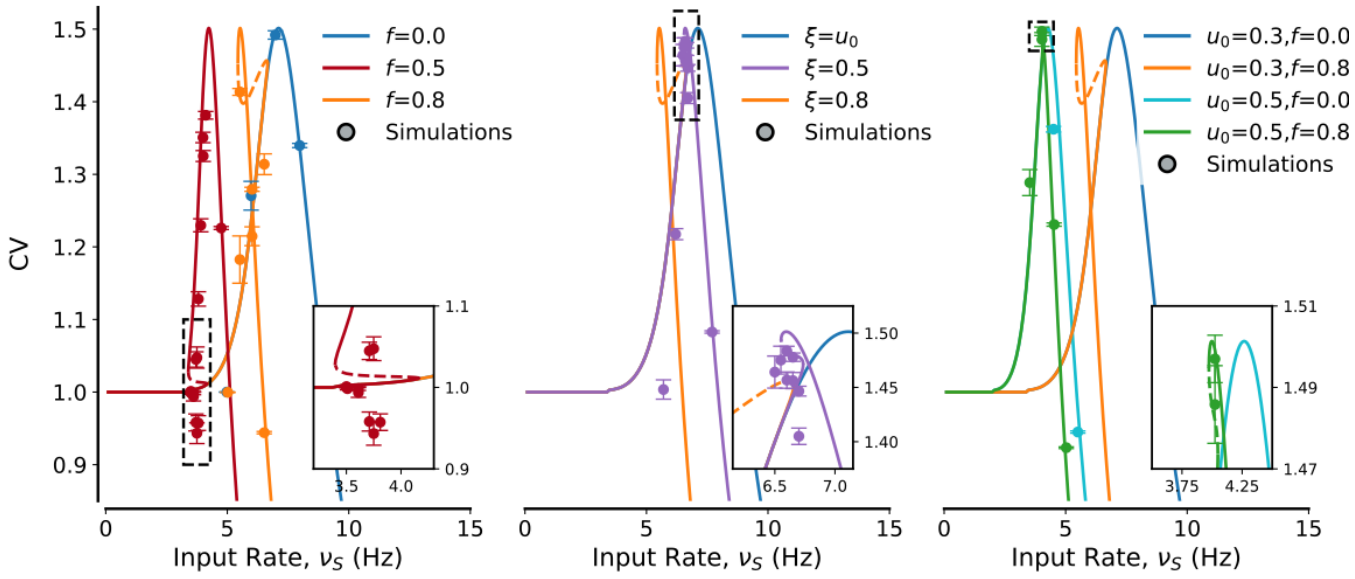

Supplementary Figure S1

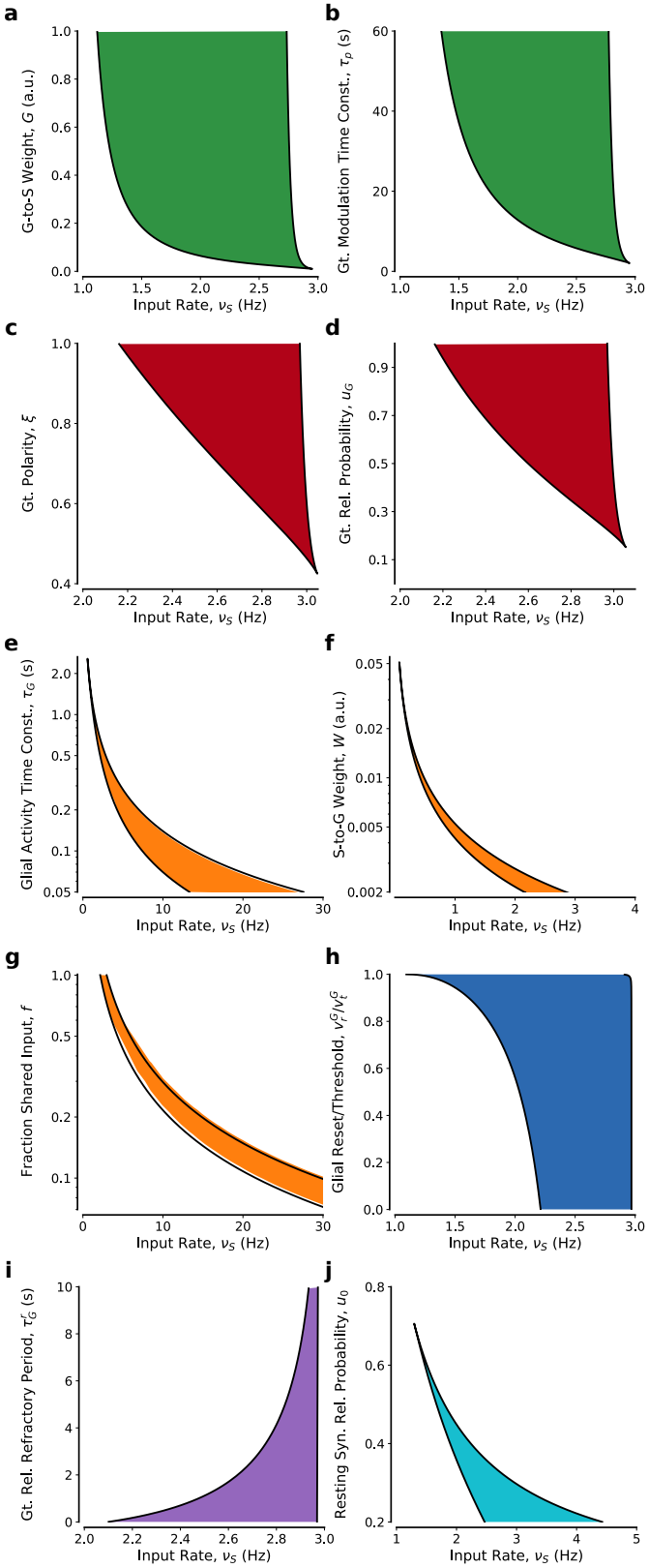

Supplementary Figure S2

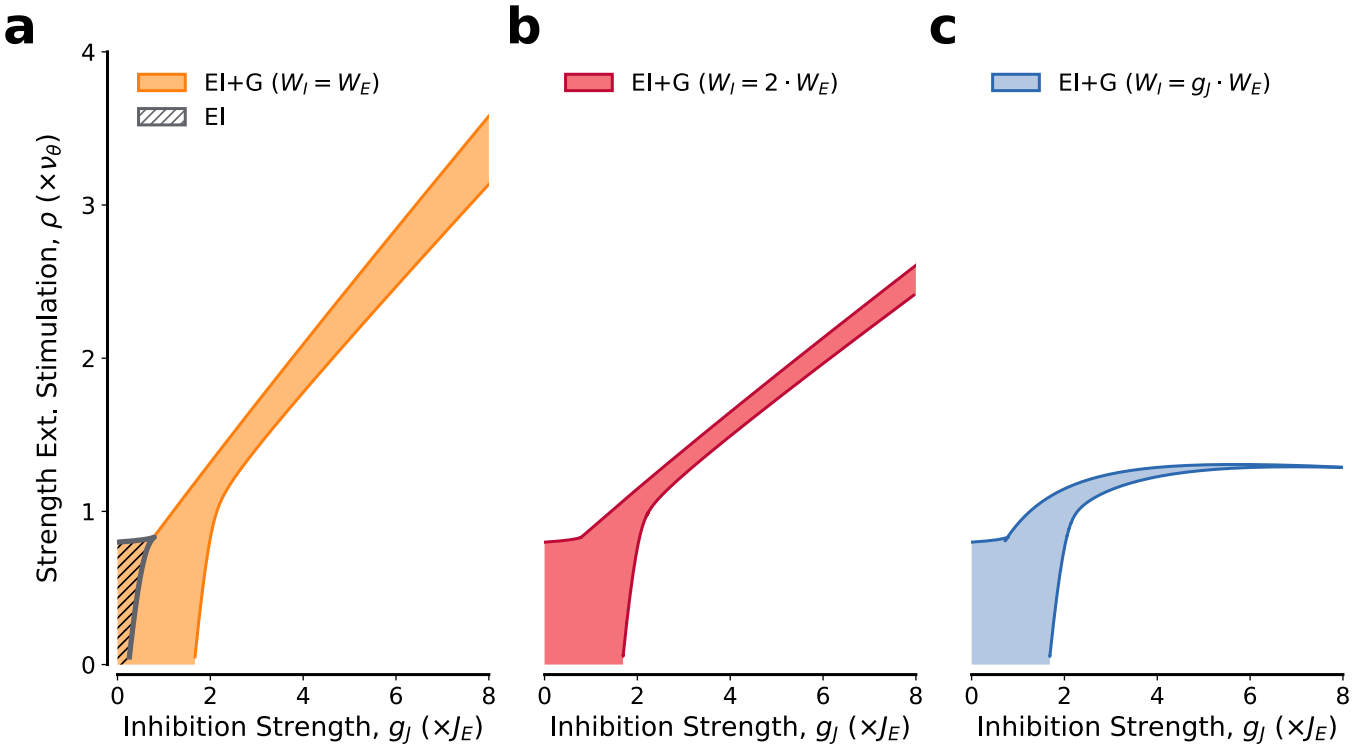

Supplementary Figure S3

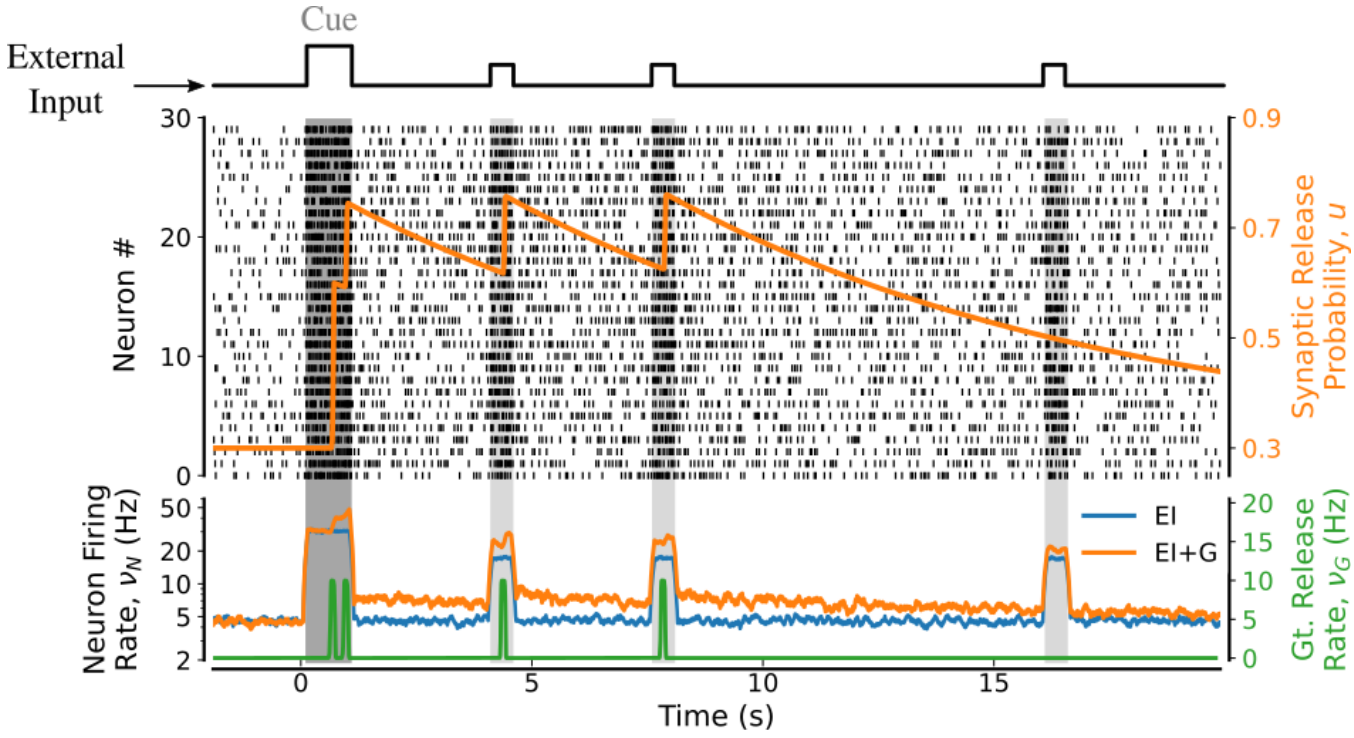

Supplementary Figure S4

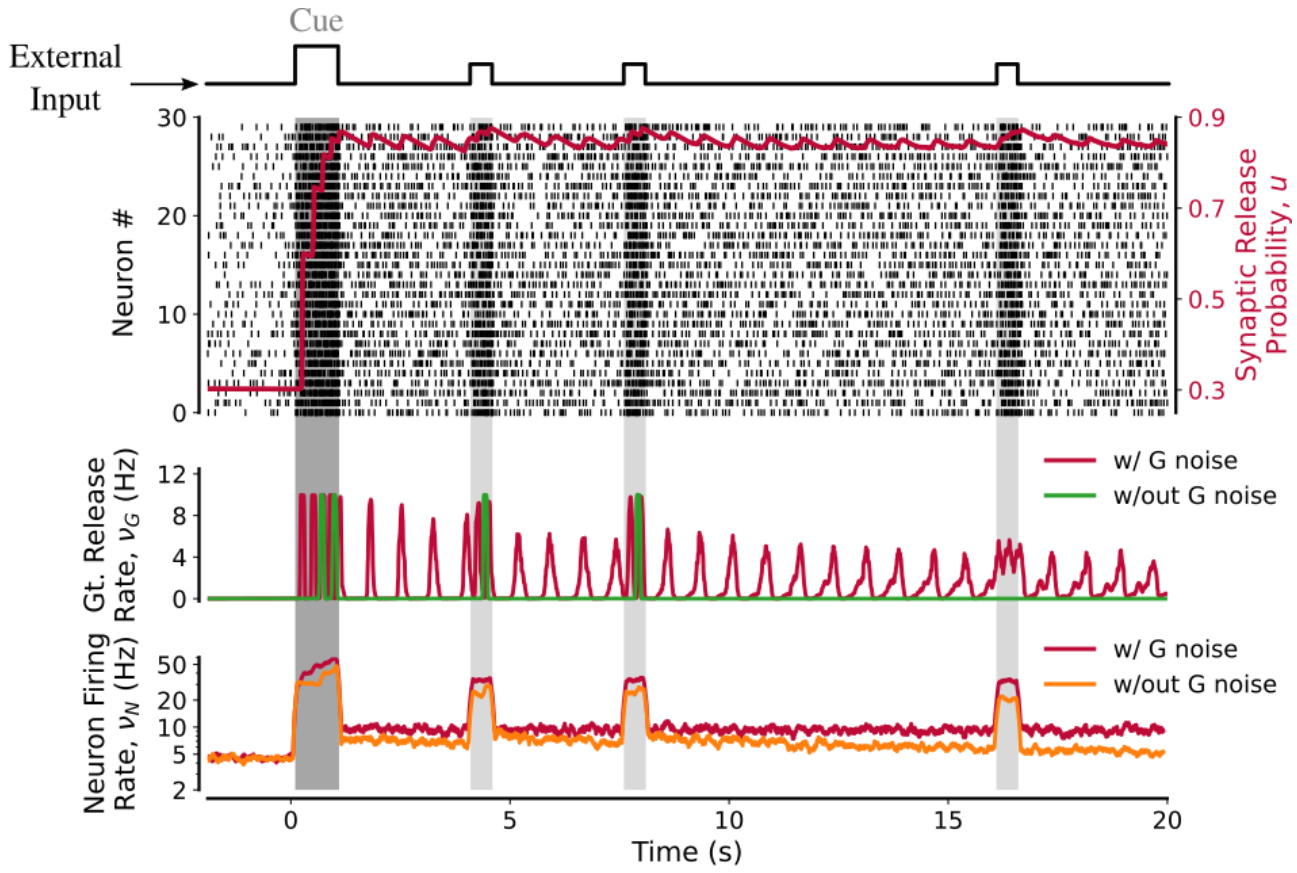

Supplementary Figure S5

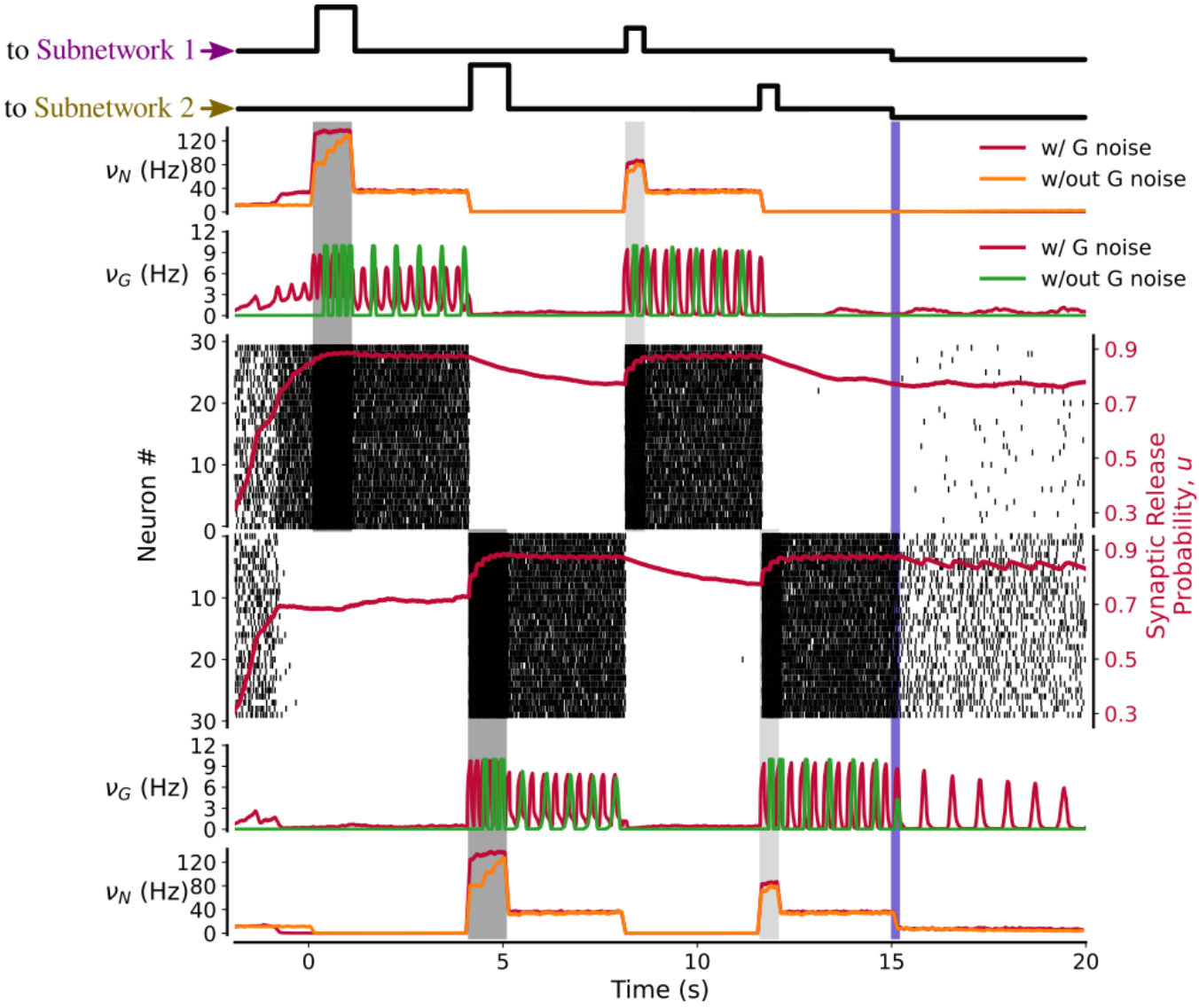

Supplementary Figure S6

References

1. A Panatier, et al., Astrocytes are endogenous regulators of basal transmission at central synapses. *Cell* **146**, 785–798 (2011).
2. G Perea, A Araque, Properties of synaptically evoked astrocyte calcium signal reveal synaptic information processing by astrocyte. *J. Neurosci.* **25**, 2192–2203 (2005).
3. W Tang, et al., Stimulation-evoked Ca^{2+} signals in astrocytic processes at hippocampal CA3–CA1 synapses of adult mice are modulated by glutamate and ATP. *J. Neurosci*. **35**, 3016–3021 (2015).
4. MD Haustein, et al., Conditions and constraints for astrocyte calcium signaling in the hippocampal mossy fiber pathway. *Neuron* **82**, 413–429 (2014).
5. E Bindocci, I Savtchouk, N Liaudet, D Becker, A Carriero, G.and Volterra, Three-dimensional Ca^{2+} imaging advances understanding of astrocyte biology. *Science* **356**, 6339 (2017).
6. L Pasti, A Volterra, T Pozzan, G Carmignoto, Intracellular calcium oscillations in astrocytes: a highly plastic, bidirectional form of communication between neurons and astrocytes *in situ*. *J. Neurosci.* **17**, 7817–7830 (1997).
7. R Zorec, et al., Astroglial excitability and gliotransmission: An appraisal of Ca^{2+} as a signaling route. *ASN Neuro* **4**, e00080 (2012).
8. A Denizot, M Arizono, UV Nägerl, H Soula, H Berry, Simulation of calcium signaling in fine astrocytic processes: Effect of spatial properties on spontaneous activity. *PLoS Comput. Biol*. **15**, e1006795 (2019).
9. Z Wang, M Tymianski, OT Jones, M Nedergaard, Impact of cytoplasmic calcium buffering on the spatial and temporal characteristics of intercellular calcium signals in astrocytes. *J. Neurosci*. **17**, 7359–7371 (1997).
10. M Jafri, J Keizer, On the roles of Ca^{2+} diffusion, Ca^{2+} buffers, and the endoplasmic reticulum in IP_3-induced Ca^{2+} waves. *Biophys. J*. **69**, 2139–2153 (1995).
11. NJ Gerkau, C Rakers, S Durry, GC Petzold, CR Rose, Reverse NCX attenuates cellular sodium loading in metabolically compromised cortex. *Cereb. Cortex* **28**, 4264–4280 (2018).
12. M Blaustein, M Juhaszova, V Golovina, P Church, E Stanley, Na/Ca exchanger and PMCA localization in neurons and astrocytes. *Annals New York Acad. Sci*. **976**, 356–366 (2002).
13. M Arizono, et al., Structural basis of astrocytic Ca^{2+} signals at tripartite synapses. *Nat. communications* **11**, 1–15 (2020).
14. JL Stobart, et al., Cortical circuit activity evokes rapid astrocyte calcium signals on a similar timescale to neurons. *Neuron* **98**, 726–735 (2018).
15. JM Gee, et al., Imaging activity in neurons and glia with a *polr2a*-based and cre-dependent GCaMP5G-IRES-tdTomato reporter mouse. *Neuron* **83**, 1058–1072 (2014).
16. J Schummers, H Yu, M Sur, Tuned responses of astrocytes and their influence on hemodynamic signals in the visual cortex. *Sci. STKE* **320**, 1638 (2008).
17. K Kanemaru, et al., In vivo visualization of subtle, transient, and local activity of astrocytes using an ultrasensitive Ca^{2+} indicator. *Cell Reports* **8**, 311–318 (2014).
18. J Marchaland, et al., Fast subplasma membrane Ca^{2+} transients control exo-endocytosis of synaptic-like microvesicles in astrocytes. *J. Neurosci.* **28**, 9122–9132 (2008).
19. E Pryazhnikov, L Khiroug, Sub-micromolar increase in $[Ca^{2+}]_i$ triggers delayed exocytosis of ATP in cultured astrocytes. *Glia* **56**, 38–49 (2008).
20. L Pasti, M Zonta, T Pozzan, S Vicini, G Carmignoto, Cytosolic calcium oscillations in astrocytes may regulate exocytotic release of glutamate. *J. Neurosci.* **21**, 477–484 (2001).
21. I Savtchouk, A Volterra, Gliotransmission: Beyond black-and-white. *J. Neurosci*. **38**, 14–25 (2018).
22. P Jourdain, et al., Glutamate exocytosis from astrocytes controls synaptic strength. *Nat. Neurosci.* **10**, 331–339 (2007).
23. DOD Mak, JK Foskett, Inositol 1,4,5-trisphosphate receptors in the endoplasmic reticulum: a single-channel point of view. *Cell calcium* **58**, 67–78 (2015).
24. M De Pittà, E Ben-Jacob, H Berry, G protein-coupled receptor-mediated calcium signaling in astrocytes in *Computational Glioscience*, eds. M De Pittà, H Berry. (Springer), p. 115–150 (2019).
25. K Pattni, G Banting, $Ins(1,4,5)P_3$ metabolism and the family of IP_3-3Kinases. *Cell. Signal*. **16**, 643–654 (2004).
26. M Morita, Y Kudo, Growth factors upregulate astrocyte $[Ca^{2+}]_i$ oscillation by increasing SERCA2b expression. *Glia* **58**, 1988–1995 (2010).
27. A Agarwal, et al., Transient opening of the mitochondrial permeability transition pore induces microdomain calcium transients in astrocyte processes. *Neuron* **93**, 587–605 (2017).
28. KS Han, et al., Channel-mediated astrocytic glutamate release via Bestrophin-1 targets synaptic NMDARs. *Mol. Brain* **6**, 1–9 (2013).
29. DH Woo, et al., TREK-1 and Best1 channels mediate fast and slow glutamate release in astrocytes upon GPCR activation. *Cell* **151**, 25–40 (2012).
30. S Lee, et al., Channel-mediated tonic GABA release from glia. *Science* **330**, 790–796 (2010).
31. X Yu, et al., Reducing astrocyte calcium signaling in vivo alters striatal microcircuits and causes repetitive behavior. *Neuron* **99**, 1170–1187 (2018).
32. M Lee, EG McGeer, PL McGeer, Mechanisms of GABA release from human astrocytes. *Glia* **59**, 1600–1611 (2011).
33. CB Giaume, CC Naus, JC Saez, L Leybaert, Glial connexins and pannexins in the healthy and diseased brain. *Physiol. Rev*. **101**, 93–145 (2021).
34. J Stehberg, et al., Release of gliotransmitters through astroglial connexin 43 hemichannels is necessary for fear memory consolidation in the basolateral amygdala. *The FASEB J*. **26**, 3649–3657 (2012).
35. HT Liu, T Akita, T Shimizu, RZ Sabirov, Y Okada, Bradykinin-induced astrocyte–neuron signalling: glutamate release is mediated by

ROS-activated volume-sensitive outwardly rectifying anion channels. *The J. Physiol*. **587**, 2197–2209 (2009).
36. LA Newman, DL Korol, PE Gold, Lactate produced by glycogenolysis in astrocytes regulates memory processing. *PloS One* **6**, e28427 (2011).
37. A Suzuki, et al., Astrocyte-neuron lactate transport is required for long-term memory formation. *Cell* **144**, 810–823 (2011).
38. H Tani, et al., A local glutamate-glutamine cycle sustains synaptic excitatory transmitter release. *Neuron* **81**, 888–900 (2014).
39. DA Sahlender, I Savtchouk, A Volterra, What do we know about gliotransmitter release from astrocytes? *Phil. Tran. R. Soc. B* **369**, 20130592 (2014).
40. M De Pittà, *Neuron-Glial Interactions*, eds. D Jaeger, R Jung. (Springer New York, New York, NY), pp. 1–30 (2020).
41. RS Zucker, WG Regehr, Short-term synaptic plasticity. *Annu. Rev. Physiol.* **64**, 355–405 (2002).
42. A Araque, et al., Gliotransmitters travel in time and space. *Neuron* **81**, 728–739 (2014).
43. M De Pittà, N Brunel, A Volterra, Astrocytes: orchestrating synaptic plasticity? *Neuroscience* (2015).
44. PS Pinheiro, C Mulle, Presynaptic glutamate receptors: physiological functions and mechanisms of action. *Nat. Rev. Neurosci.* **9**, 423–436 (2008).
45. R Cunhaa, J Ribeiro, ATP as a presynaptic modulator. *Life Sci.* **68**, 119–137 (2000).
46. M De Pittà, Gliotransmitter exocytosis and its consequences on synaptic transmission in *Computational Glioscience*, eds. M De Pittà, H Berry. (Springer), p. 245–287 (2019).
47. W Gerstner, WM Kistler, R Naud, L Paninski, *Neuronal dynamics: From single neurons to networks and models of cognition*. (Cambridge University Press), (2014).
48. AJ Siegert, On the first passage time probability problem. *Phys. Rev*. **81**, 617 (1951).
49. LM Ricciardi, *Diffusion processes and related topics in Biology*. (Springer Science & Business Media) Vol. 14, (1977).
50. DJ Amit, MV Tsodyks, Quantitative study of attractor neural network retrieving at low spike rates: I. Substrate-spikes, rates and neuronal gain. *Network* **2**, 259–273 (1991).
51. S Ostojic, N Brunel, From spiking neuron models to linear-nonlinear models. *PLoS Comput. Biol*. **7**, e1001056 (2011).
52. N Brunel, Dynamics of sparsely connected networks of excitatory and inhibitory spiking neurons. *J. Comput. Neurosci.* **8**, 183–208 (2000).
53. F Barbieri, N Brunel, Irregular persistent activity induced by synaptic excitatory feedback. *Front. Comp. Neurosci.* **1**, P167 (2007).
54. D Amit, N Brunel, Model of global spontaneous activity and local structured activity during delay periods in the cerebral cortex. *Cereb. Cortex* **7**, 237–252 (1997).
55. S Herculano-Houzel, B Mota, R Lent, Cellular scaling rules for rodent brains. *Proc. Natl. Acad. Sci*. **103**, 12138–12143 (2006).
56. J Bahney, CS von Bartheld, Validation of the isotropic fractionator: comparison with unbiased stereology and DNA extraction for quantification of glial cells. *J. Neurosci. Methods* **222**, 165–174 (2014).
57. S Herculano-Houzel, CS von Bartheld, DJ Miller, JH Kaas, How to count cells: the advantages and disadvantages of the isotropic fractionator compared with stereology. *Cell Tissue Res*. **360**, 29–42 (2015).
58. C Calì, et al., 3D cellular reconstruction of cortical glia and parenchymal morphometric analysis from Serial Block-Face Electron Microscopy of juvenile rat. *Prog. Neurobiol*. **183**, 101696 (2019).
59. EA Bushong, ME Martone, YZ Jones, MH Ellisman, Protoplasmic astrocyte in CA1 stratum radiatum occupy separate anatomical domains. *J. Neurosci.* **22**, 183–192 (2002).
60. L Abdeladim, et al., Multicolor multiscale brain imaging with chromatic multiphoton serial microscopy. *Nat. Commun*. **10**, 1–14 (2019).
61. N Kasthuri, et al., Saturated reconstruction of a volume of neocortex. *Cell* **162**, 648–661 (2015).
62. C Genoud, GW Knott, K Sakata, B Lu, E Welker, Altered synapse formation in the adult somatosensory cortex of brain-derived neurotrophic factor heterozygote mice. *J. Neurosci*. **24**, 2394–2400 (2004).
63. M Santello, P Bezzi, A Volterra, TNFα controls glutamatergic gliotransmission in the hippocampal dentate gyrus. *Neuron* **69**, 988–1001 (2011).
64. M Corkrum, et al., Dopamine-evoked synaptic regulation in the nucleus accumbens requires astrocyte activity. *Neuron* **105**, 1036–1047 (2020).
65. A Covelo, A Araque, Neuronal activity determines distinct gliotransmitter release from a single astrocyte. *eLife* **7**, e32237 (2018).
66. M Navarrete, et al., Astrocytes mediate in vivo cholinergic-induced synaptic plasticity. *PLoS Biol*. **10**, e1001259 (2012).
67. JGG Borst, The low synaptic release probability in vivo. *Trends Neurosci*. **33**, 259–266 (2010).
68. JY Yoon, HR Lee, WK Ho, SH Lee, Disparities in short-term depression among prefrontal cortex synapses sustain persistent activity in a balanced network. *Cereb. Cortex* **30**, 113–134 (2020).
69. T Takano, et al., Chemico-genetic discovery of astrocytic control of inhibition *in vivo*. *Nature* pp. 1–7 (2020).
70. M Martin-Fernandez, et al., Synapse-specific astrocyte gating of amygdala-related behavior. *Nat. Neurosci*. **20**, 1540 (2017).
71. A Serrano, N Haddjeri, J Lacaille, R Robitaille, GABAergic network activation of glial cells underlies heterosynaptic depression. *J. Neurosci.* **26**, 5370–5382 (2006).
72. J Kang, L Jiang, SA Goldman, M Nedergaard, Astrocyte-mediated potentiation of inhibitory synaptic transmission. *Nat. Neurosci.* **1**, 683–692 (1998).